Lithos 120 (2010) 529–546

Contents lists available at ScienceDirect

Lithos

journal homepage: www.elsevier.com/locate/lithos

Petrogenesis of late Triassic post-collisional basaltic rocks of the Lancangjiang tectonic zone, southwest China, and tectonic implications for the evolution of the eastern Paleotethys: Geochronological and geochemical constraints

Yuejun Wang [a,*], Aimei Zhang [a], Weiming Fan [a], Touping Peng [a], Feifei Zhang [a], Yanhua Zhang [b], Xiawu Bi [c]

[a] Key Laboratory of Isotope Geochronology and Geochemistry, Guangzhou Institute of Geochemistry, Chinese Academy of Sciences, Guangzhou 510640, China
[b] CSIRO Earth Science and Resource Engineering, P.O. Box 1130, Bentley, WA 6102, Australia
[c] Institute of Geochemistry, Chinese Academy of Sciences, Guiyang, China

ARTICLE INFO

Article history:
Received 22 June 2010
Accepted 16 September 2010
Available online 13 October 2010

Keywords:
Elemental and isotopic geochemistry
Zircon U–Pb geochronology
Late Triassic post-collisional magmatism
Lancangjiang tectonic zone
Eastern Paleotethys
Southwestern China

ABSTRACT

The Xiaodingxi and Manghuihe volcanic sequences represent key components of the Lancangjiang igneous zone in southwest China. Their petrogenesis provides important constraints on the tectonic evolution of the eastern Paleotethys ocean. The basaltic rocks from the Xiaodingxi and Manghuihe sequences yield SHRIMP zircon U–Pb weighted mean ages of 214 ± 7 Ma and 210 ± 22 Ma, respectively, which is 15–20 Ma younger than the ages of the syn-collisional granite magmatism (230–241 Ma). Samples from the volcanic sequences are dominated by alkaline basalts and basaltic andesites, and can be geochemically classified into two groups. Group 1 samples, mainly from the Xiaodingxi sequence and the lower part of the Manghuihe sequence, are characterized by low MgO (1.49–7.50 wt.%) and Zr/Nb (9.4–15.3), and high Al_2O_3 (15.95–18.39 wt.%). They are enriched in LILE and LREE contents and depleted in HFSE, and have $^{87}Sr/^{86}Sr(t)$ ratios of 0.705473–0.706972, $\varepsilon_{Nd}(t)$ of −1.47–0.75, and similar Pb isotopic compositions to the global average composition of pelagic sediments. In contrast, Group 2 samples from the middle–upper parts of the Manghuihe sequence have similar Al_2O_3 (16.62–18.23 wt.%) but higher MgO (8.08–11.74 wt.%) and Zr/Nb (15.9–23.9) than those of Group 1 samples. They exhibit relatively flat REE patterns, significantly negative Nb–Ta and Th–U anomalies and positive Sr anomalies. In comparison with Group 1, Group 2 samples show higher Cr, Ni contents and $\varepsilon_{Nd}(t)$ values (1.17–5.02), and lower $^{87}Sr/^{86}Sr(t)$ and Pb isotopic ratios ($\Delta 8/4 = 43.2–59.8$ and $\Delta 7/4 = 11.8–19.8$). The geochemical data suggest that Group 1 samples might be the differentiated product of primitive high MgO and low Al_2O_3 melts originating from a refractory modified mantle with the involvement of 5–10% recycled pelagic sediments. The parental magma for Group 2 samples may have been derived from a plagioclase-rich, garnet-free source comprising 80–85% fluid-metasomatized and 15–20% asthenospheric components. Based on all available data, a tectonic model involving eastward subduction in the Permian and collision in the Triassic can be proposed for the evolution of the eastern Paleotethys ocean. During the late Triassic, the progressive upwelling of the asthenospheric mantle, shortly after slab detachment, may have led to the melting of the metasomatized mantle wedge, resulting in the post-collisional Group 1 and Group 2 magmas.
© 2010 Elsevier B.V. All rights reserved.

1. Introduction

A record of the late Paleozoic to Mesozoic Paleotethys ocean is preserved in rock sequences extending from the Alps through Afghanistan to southwestern China and in Peninsular Malaysia (Bullard et al., 1965; Hsu and Bernoulli, 1978; Sengor and Hsu, 1984; Metcalfe, 1996; Acharyya, 1998; Metcalfe, 2002). The inferred eastern segment of the ocean include the Bentong–Raub zone in Peninsular Malaysia, the Inthanon suture in northwestern Thailand and the Lancangjiang tectonic zone in southwestern China from south to north (Fig. 1a; e.g., Hutchison, 1989; Fan and Zhang, 1994; Wu et al., 1995; Metcalfe, 1996, 2002). The Lancangjiang tectonic zone separates the Simao from Baoshan Bocks during the Paleozoic period. The tectonic zone is regarded as a key element in studying the evolution of the Paleotethys due to its preservation of ocean remnants, including, mélange, ophiolite suite, oceanic basalts, radiolarian-bearing silicalite, high-pressure metamorphic rocks, blueschist and associated arc-magmatism (e.g., Sengor, 1979; Sengor and Hsu, 1984; Metcalfe, 1996; Zhong, 1998; Tabakh and Utha-Aroon, 1998; Mo et al., 1998; Metcalfe, 2002; Feng, 2002; Fontaine, 2002; Peng et al., 2008; Jian et al., 2009; Hennig et al., 2009).

Previous studies on the Lancangjiang tectonic zone focused largely on the reconstruction of biostratigraphical and ecological patterns

* Corresponding author. Guangzhou Institute of Geochemistry, Chinese Academy of Sciences, P.O. Box 1131, Guangzhou 510640, China. Tel.: +86 20 85290527.
E-mail address: yjwang@gig.ac.cn (Y. Wang).

0024-4937/$ – see front matter © 2010 Elsevier B.V. All rights reserved.
doi:10.1016/j.lithos.2010.09.012

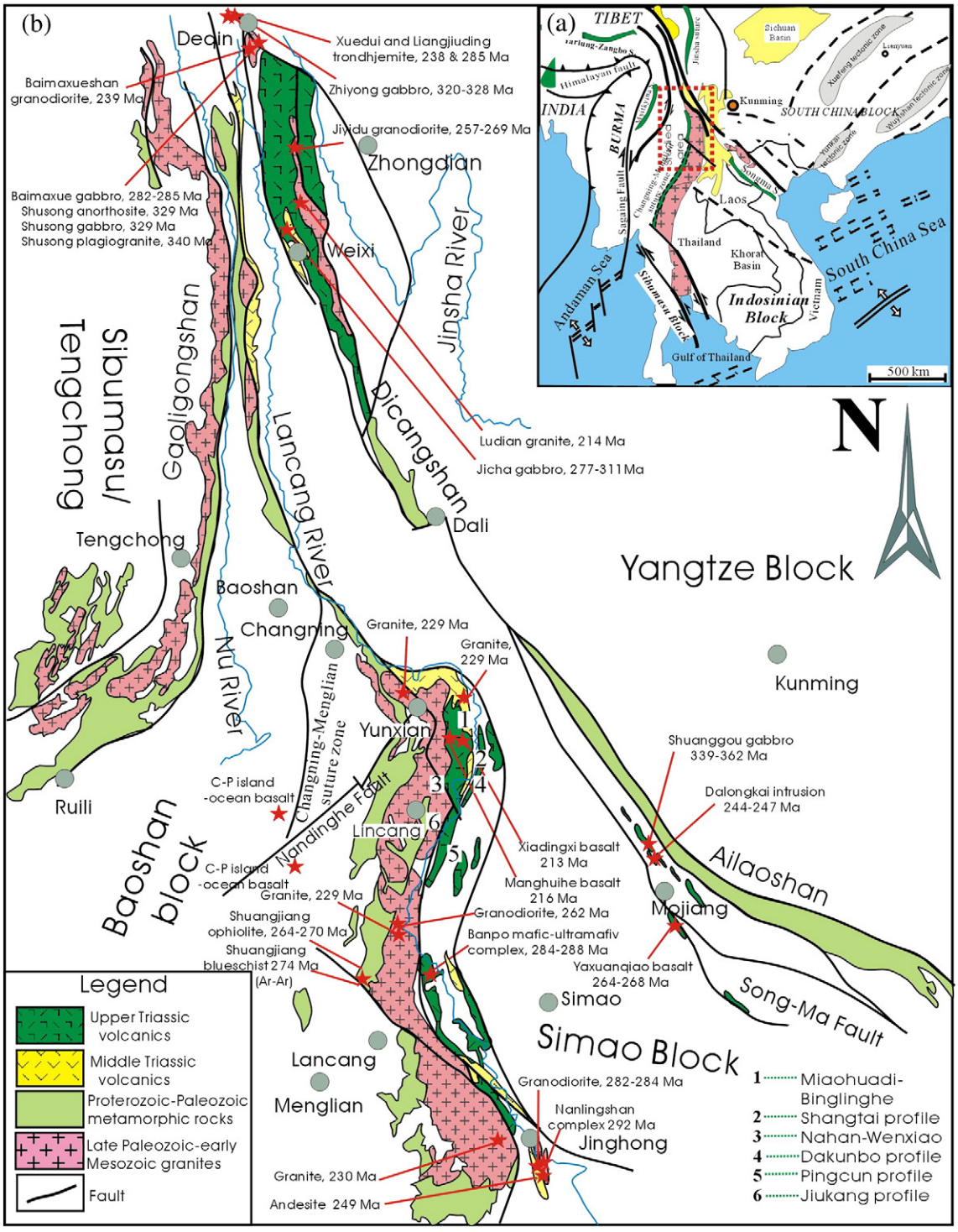

Fig. 1. (a) Tectonic outline of Southeast Asia and (b) simplified geological map of the Lancangjiang tectonic zone in southwest China.

within the ocean (e.g., Mo et al., 1998; Zhong, 1998; Jian et al., 2009). Much less attention has been focused on the petrogenesis of the Permian–Triassic volcanic zone (Fig. 1a–b; e.g., Yunnan BGMR, 1990; Mo et al., 1998; Zhong, 1998; Peng et al., 2008). The preserved remnants of the volcanic zone extend more than 400 km along the Lancangjiang River, and constitute part of a broader igneous belt, linking to the north with the Weixi–Deqin–Yushu igneous zone in eastern Tibet and toward the south with the Chiang Khong–Tak volcanic zones in southwestern Thailand (Fig. 1a, Yunnan BGMR, 1990; Mo et al., 1998; Zhong, 1998; Barr et al., 2000; Panjasawatwong et al., 2006).

Previous studies on the volcanic rocks (e.g., Yunnan BGMR, 1990; Mo et al., 1998; Zhong, 1998; Hou et al., 2003) have generated lithofacies and lithochemical data but the age of the units is poorly constrained. Several different ages have been proposed, including the latest Permian, late Permian to early Triassic and middle Triassic–early Jurassic (e.g., Cobbing et al., 1992; Mo et al., 1998; Zhong, 1998; Hou et al., 2003; Peng et al., 2008). The tectonic setting of these rocks has also been debated, with several different proposals including oceanic, subduction, syn- and post-collisional and intracontinental settings (Macdonald and Barr, 1978; Liu et al., 1989; Barr et al., 2000; Mo et al., 1998; Zhong, 1998; Phajuy et al., 2005; Panjasawatwong et al., 2006;

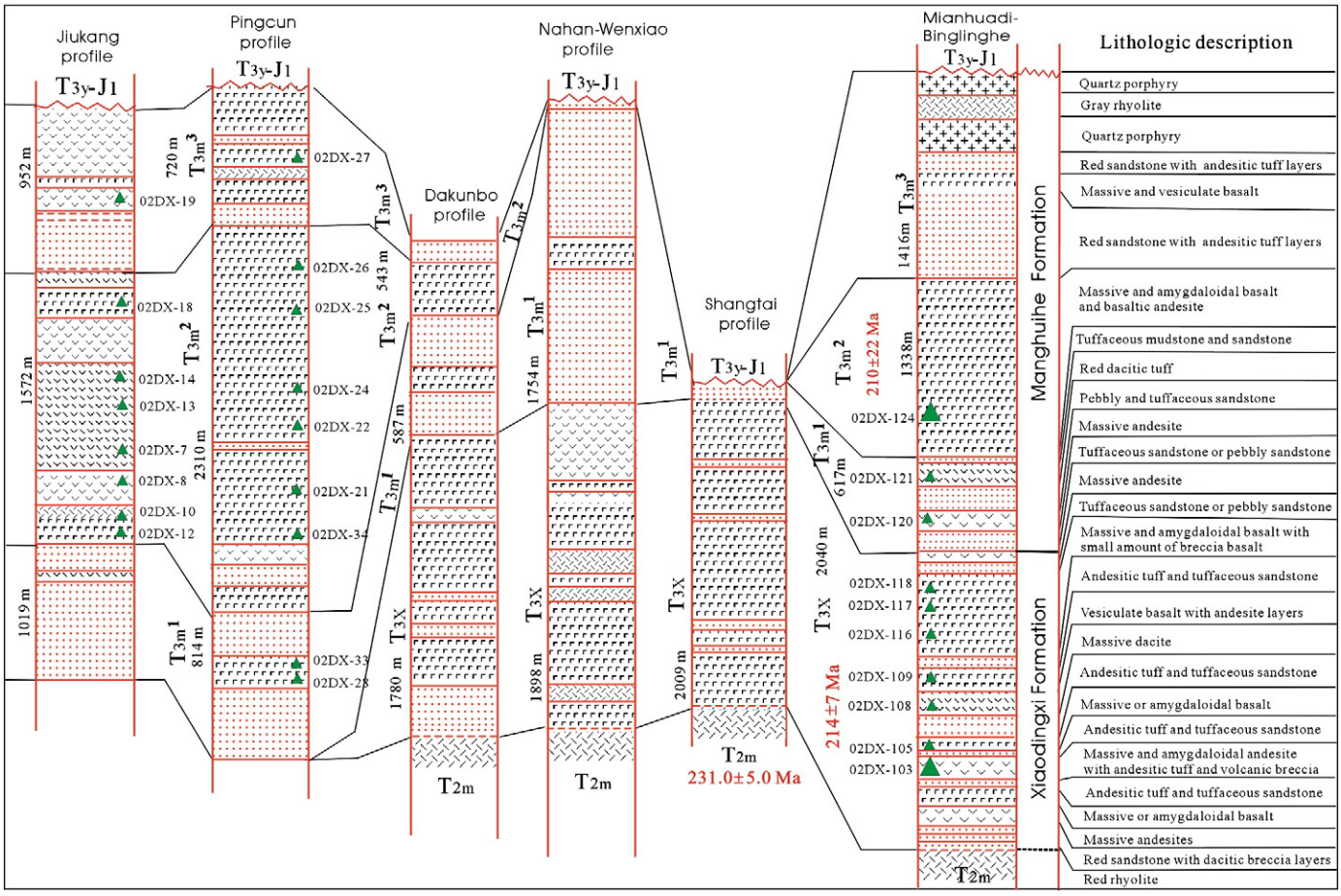

Fig. 2. (b) Typical volcanic sections of the upper Triassic Xiaodingxi and Manghui formations including the Jiukang, Pingcun, Dakunbo, Nahan–Wenjiao, Shangtai and Mianhuadi–Binglinghe sections. Sampled locations are marked.

Peng et al., 2008). These uncertainties in the tectonic evolution of Paleotethys largely reflect the poor understanding of the petrology, geochronology and geochemistry (elemental and Sr–Nd–Pb isotopic compositions) of the volcanic rocks.

The currently available data show that the volcanic sequences along the Lancangjiang tectonic zone are composed of the intermediate–felsic Manghua Formation, and the intermediate–mafic Xiaodingxi and Manghuihe formations. In this study, six sections through the

Table 1
SHRIMP zircon U–Pb analytical results for typical samples from the Xiaodingxi and Manghuihe formations.

Spots	U (ppm)	Th (ppm)	Th/U	Pb (ppm)	Common ^{206}Pb (10^{-2})	$^{206}Pb/^{238}U$ ($\pm1\sigma$)	$^{207}Pb/^{235}U$ ($\pm1\sigma$)	$^{207}Pb/^{206}Pb$ ($\pm1\sigma$)	$^{206}Pb/^{238}U \pm 1\sigma$ (Ma)
02DX-103 (basaltic andesite, Xiaodingxi formation)									
G1	188	113	0.60	7.1	0.70	0.0342 ± 1.5	0.3190 ± 2.9	0.0676 ± 5.0	216.8 ± 9.1
G2	149	941	0.63	6.2	1.19	0.0326 ± 1.6	0.3883 ± 6.7	0.0865 ± 13.9	206.5 ± 10.0
G3	719	501	0.70	26.1	0.21	0.0319 ± 1.3	0.2623 ± 1.8	0.0596 ± 2.9	202.5 ± 8.4
G4	970	313	0.32	34.8	0.14	0.0357 ± 1.3	0.2669 ± 1.3	0.0542 ± 1.5	226.0 ± 8.2
G5	293	121	0.41	10.0	0.43	0.0325 ± 1.3	0.2887 ± 3.2	0.0644 ± 6.2	206.2 ± 8.4
G6	472	151	0.32	13.9	0.16	0.0287 ± 1.1	0.2303 ± 1.4	0.0581 ± 2.3	182.6 ± 7.1
G7	1284	500	0.39	49.0	0.19	0.0374 ± 1.9	0.2739 ± 1.7	0.0531 ± 1.7	236.7 ± 12.0
G8	173	118	0.68	7.1	2.65	0.0320 ± 1.7	0.3585 ± 8.2	0.0812 ± 17.5	203.2 ± 10.6
G9	650	154	0.24	23.0	0.21	0.0347 ± 1.4	0.2920 ± 2.1	0.0611 ± 3.3	219.8 ± 8.9
G10	682	250	0.37	34.9	1.83	0.0499 ± 4.7	0.3517 ± 8.1	0.0511 ± 10.1	314.0 ± 29.0
G11	1104	161	0.15	43.1	0.57	0.0408 ± 2.3	0.3156 ± 3.3	0.0561 ± 4.5	257.9 ± 14.0
G12	453	173	0.38	16.0	0.75	0.0324 ± 1.2	0.3174 ± 3.0	0.0712 ± 5.9	205.2 ± 7.8
G13	676	481	0.71	26.9	0.94	0.0351 ± 1.5	0.3013 ± 2.9	0.0622 ± 5.0	222.6 ± 9.6
02DX-124 (basaltic andesite, Manghuihe formation)									
F1	1972	1252	0.66	55.3	0.77	0.0324 ± 4.9	0.218 ± 5.4	0.0488 ± 2.4	205.5 ± 9.8
F2	1251	883	0.73	33.4	0.39	0.0310 ± 4.9	0.221 ± 5.3	0.0516 ± 2.1	196.8 ± 9.4
F3	871	148	0.17	70.2	0.30	0.0390 ± 4.9	0.266 ± 5.1	0.0496 ± 1.5	246.0 ± 12.0
F4	1573	995	0.65	45.9	0.35	0.0338 ± 4.9	0.240 ± 5.8	0.0514 ± 3.1	214.0 ± 10.0
F5	462	343	0.77	16.1	0.91	0.0479 ± 5.0	0.266 ± 7.0	0.0403 ± 4.9	254.0 ± 2.0
F6	695	109	0.16	21.8	0.30	0.0364 ± 4.9	0.253 ± 5.5	0.0504 ± 2.5	231.0 ± 11.0
F7	709	98	0.14	30.4	1.60	0.0528 ± 5.2	0.358 ± 7.1	0.0492 ± 4.9	310.0 ± 15.0

Data processing was carried out using the SQUID 1.03 and Isoplot/Ex 2.49 programs of Ludwig (2001).

Table 2
Major, trace element abundances and Sr–Nd isotopic compositions for typical samples from the Xiaodingxi and Manghuihe formations.

Sample	02DX-12	02DX-28	02DX-33	02DX-103	02DX-105	02DX-108	02DX-109	02DX-116	02DX-117	02DX-118	02DX-120	02DX-121	02DX-124
	Group 1												
	Manghuihe formation			Xiaodingxi formation							Manghuihe formation		
	Jiukang	Pingcun section		Xiaodingxi section									
SiO_2	53.29	53.57	52.68	50.45	49.65	45.86	46.36	46.23	47.65	45.94	46.15	47.47	53.64
TiO_2	1.15	1.17	1.19	1.56	1.43	2.14	1.92	2.10	2.11	2.11	2.27	2.10	0.81
Al_2O_3	16.85	16.29	16.20	15.36	16.63	15.30	16.43	15.45	15.68	16.66	15.43	15.52	17.11
MgO	4.97	5.20	5.67	4.39	4.86	6.70	6.13	7.11	6.14	6.54	6.40	6.80	1.39
Fe_2O_3	5.26	3.90	2.90	2.66	2.74	5.38	6.32	5.13	4.85	5.18	7.77	4.41	2.54
FeO	2.82	4.33	5.22	6.17	5.10	7.02	5.88	6.93	6.58	6.68	5.07	7.18	2.97
CaO	2.72	7.42	4.83	6.30	5.33	7.73	7.59	6.07	7.19	5.88	6.05	4.36	5.41
K_2O	2.72	2.31	3.90	2.06	4.33	1.95	2.01	2.57	2.44	2.61	2.92	2.74	5.11
Na_2O	5.55	3.08	3.18	3.67	3.30	2.73	2.49	2.12	2.72	2.72	2.77	3.53	3.73
P_2O_5	0.41	0.47	0.49	0.50	0.59	0.92	0.88	0.67	0.71	0.78	0.73	0.97	0.23
MnO	0.46	0.15	0.20	0.19	0.16	0.22	0.18	0.39	0.17	0.34	0.31	0.38	0.08
LOI	3.35	1.91	3.30	6.46	5.68	3.83	3.57	3.91	3.55	4.26	3.78	4.28	6.80
Total	99.55	99.80	99.76	99.77	99.80	99.78	99.76	98.68	99.79	99.70	99.65	99.74	99.82
Sc	21.3	21.2	20.6	20.8	20.4	26.2	24.7	28.1	28.7	28.0	28.0	30.0	12.7
V	151.8	146.4	142.0	143.2	152.6	203.0	197.7	227.4	221.1	216.0	224.3	228.8	117.5
Cr	97.4	133.8	134.4	54.9	10.1	160.1	157.7	174.3	170.9	167.8	176.9	118.3	20.3
Co	21.4	24.6	24.4	21.1	17.5	32.8	30.8	35.4	31.9	30.5	37.5	30.1	4.5
Ni	39.1	53.5	54.7	25.9	4.2	49.9	60.7	48.5	48.3	39.2	59.8	32.7	6.0
Rb	91.3	63.2	108.8	59.1	251.2	69.8	81.1	140.5	106.5	97.5	103.7	76.2	194.0
Sr	332	405	299	347	234	339	454	317	287	330	435	169	95
Y	27.40	30.76	29.97	23.36	34.40	35.08	31.97	30.34	32.24	34.45	31.89	36.20	17.63
Zr	221	251	249	234	285	294	273	228	235	260	247	275	193
Nb	14.73	16.36	16.13	17.64	21.65	30.47	29.39	19.25	18.65	22.63	20.70	29.16	12.75
Cs	2.03	1.81	1.60	4.38	9.95	2.47	4.07	11.87	5.27	11.51	3.28	3.25	5.50
Ba	240	593	950	719	499	617	539	1458	508	1147	1350	859	766
La	35.13	42.10	41.94	43.01	45.42	46.46	45.84	31.29	32.19	36.88	31.57	47.24	49.70
Ce	71.44	83.27	83.36	82.60	99.90	95.79	95.14	68.14	71.00	80.99	70.45	104.59	88.57
Pr	8.55	9.81	9.73	9.68	12.76	11.96	11.56	8.73	8.97	10.48	8.86	13.14	9.62
Nd	31.51	37.12	36.77	37.29	50.04	47.10	45.83	35.87	37.95	42.59	37.64	52.50	33.67
Sm	6.13	7.01	6.82	6.27	9.23	8.87	8.35	7.28	7.62	8.63	7.54	10.15	5.52
Eu	1.71	1.93	1.91	2.00	2.20	2.83	2.71	2.35	2.41	2.66	2.47	2.49	1.37
Gd	5.88	6.95	6.85	6.34	8.90	8.69	8.19	6.94	7.60	8.37	7.47	9.30	4.76
Tb	0.93	1.03	0.97	0.85	1.26	1.25	1.22	1.06	1.11	1.25	1.07	1.29	0.74
Dy	5.16	5.27	5.26	4.52	6.53	6.54	6.03	5.79	6.25	6.70	6.27	7.20	3.23
Ho	1.04	1.13	1.14	0.92	1.36	1.31	1.21	1.16	1.24	1.34	1.23	1.42	0.65
Er	2.88	3.19	3.19	2.27	3.65	3.55	3.37	3.28	3.54	3.57	3.56	3.78	1.80
Tm	0.43	0.48	0.49	0.34	0.53	0.53	0.48	0.47	0.50	0.53	0.50	0.52	0.24
Yb	2.81	2.90	2.82	2.07	3.18	3.01	2.77	2.86	2.93	3.31	3.12	3.21	1.57
Lu	0.42	0.44	0.44	0.30	0.50	0.47	0.45	0.42	0.46	0.47	0.47	0.49	0.25
Hf	5.20	5.48	5.29	4.88	6.35	5.91	5.37	4.99	5.05	5.68	5.44	6.15	4.79
Ta	0.94	1.19	1.15	1.20	1.49	1.87	1.76	1.23	1.21	1.47	1.31	1.73	1.06
Pb	11.97	7.71	9.59	4.58	8.88	12.32	10.13	12.06	13.96	19.22	16.74	13.58	8.70
Th	9.19	9.82	9.69	6.62	15.99	3.12	3.42	2.66	3.01	4.78	2.74	4.29	15.24
U	1.99	2.10	2.08	1.49	3.96	0.79	0.85	0.68	0.78	1.22	0.73	1.05	3.18
$^{147}Sm/^{144}Nd$	0.118	0.114	0.112	0.102	0.112	0.114	0.11	0.123	0.121	0.105	0.099	0.121	0.117
$^{87}Rb/^{86}Sr$	0.798	0.453	1.054	0.493	3.106	0.596	0.518	1.285	1.076	0.611	5.938	0.691	1.308
$^{143}Nd/^{144}Nd \pm 2\sigma$	0.512514 ± 10	0.512558 ± 9	0.512519 ± 9	0.512426 ± 10	0.512444 ± 12	0.512485 ± 9	0.512486 ± 10	0.512524 ± 9	0.512482 ± 9	0.512471 ± 9	0.512424 ± 8	0.512485 ± 11	0.512474 ± 9
$^{87}Sr/^{86}Sr \pm 2\sigma$	0.709455 ± 11	0.707654 ± 11	0.709339 ± 13	0.708374 ± 17	0.716690 ± 14	0.708270 ± 14	0.707093 ± 13	0.710291 ± 16	0.709340 ± 13	0.708354 ± 13	0.725429 ± 16	0.708453 ± 13	0.709641 ± 13
$(^{87}Sr/^{86}Sr)i$	0.706959	0.706237	0.706041	0.70683	0.706972	0.706405	0.705473	0.70627	0.705974	0.706442	0.706848	0.70629	0.705549
$\varepsilon_{Nd}(t)$	−0.2	0.75	0.04	−1.47	−1.38	−0.67	−0.54	−0.15	−0.92	−0.70	−1.44	−0.87	−0.96

Chondrite uniform reservoir values, $^{147}Sm/^{144}Nd = 0.1967$, $^{143}Nd/^{144}Nd = 0.512638$, are used for the calculation. $\varepsilon_{Nd}(t)$ is calculated by assuming 215 Ma for these samples. Sm, Nd, Rb, and Sr: ppm.

Table 2 (*continued*)

Sample	02DX-7	02DX-8	02DX-10	02DX-13	02DX-14	02DX-18	02DX-19	02DX-21	02DX-22	02DX-24	02DX-25	02DX-26	02DX-27	02DX-34
	Group 2													
	Manghuihe formation													
	Jiukang section							Pingcun section						
SiO_2	48.40	47.66	48.35	47.30	44.33	45.52	47.08	45.59	46.33	46.55	45.44	47.49	45.87	44.85
TiO_2	1.09	1.05	1.05	0.85	0.85	0.85	0.89	1.35	1.23	1.34	1.21	1.33	1.30	1.27
Al_2O_3	16.83	17.04	15.82	16.03	16.15	17.19	17.07	16.25	16.71	16.19	16.18	16.05	16.04	16.58
MgO	7.95	8.91	8.49	11.00	10.52	10.21	9.11	7.74	8.85	7.89	8.24	7.87	7.92	10.34
Fe_2O_3	3.62	2.61	6.22	2.34	2.76	3.40	3.52	3.77	2.82	3.44	3.53	3.19	3.57	2.85
FeO	6.32	6.65	4.23	7.02	8.07	6.57	6.30	6.68	7.35	6.77	6.40	6.10	6.87	7.67
CaO	4.68	5.10	3.10	4.27	7.01	6.41	6.22	9.82	6.39	8.78	10.40	8.45	9.36	6.83
K_2O	2.23	2.05	4.52	0.26	0.35	0.61	0.53	1.45	1.68	1.52	1.42	0.37	1.42	0.44
Na_2O	3.59	3.18	2.69	4.36	3.10	3.13	3.67	2.64	3.05	2.78	2.37	4.06	2.83	3.20
P_2O_5	0.32	0.29	0.23	0.08	0.09	0.09	0.09	0.17	0.15	0.16	0.14	0.20	0.16	0.16
MnO	0.33	0.36	0.46	0.20	0.21	0.32	0.30	0.31	0.26	0.25	0.22	0.38	0.29	0.24
LOI	4.35	4.77	4.35	6.11	6.37	5.46	4.94	3.98	4.90	3.87	4.24	4.32	4.13	5.33
Total	99.71	99.67	99.51	99.82	99.81	99.76	99.72	99.75	99.72	99.54	99.79	99.81	99.76	99.76
Sc	28.8	29.1	31.6	33.5	35.0	33.5	35.5	36.0	32.0	34.8	34.1	31.8	36.3	33.2
V	178.6	165.9	174.1	157.4	172.6	161.1	163.6	217.9	195.2	208.1	201.4	201.9	219.5	202.3
Cr	153.8	161.2	194.5	272.8	293.0	220.4	227.6	244.2	238.6	267.9	236.0	237.6	267.0	229.4
Co	34.5	33.1	33.4	49.0	50.7	43.5	42.2	38.9	40.5	37.2	41.1	35.2	41.6	44.3
Ni	80.5	83.0	70.7	181.6	202.0	104.2	100.1	83.5	88.7	86.9	86.3	73.9	79.2	91.1
Rb	81.0	77.2	134.6	6.6	9.6	29.2	21.0	60.6	43.6	73.2	60.1	8.2	57.7	13.5
Sr	442	438	602	163	194	363	551	354	585	380	273	278	383	529
Y	23.65	21.68	22.72	20.83	22.13	20.80	21.29	22.89	22.32	23.16	21.48	22.77	23.43	22.44
Zr	130	124	107	58	60	65	66	93	85	97	87	107	99	92
Nb	8.18	7.47	6.06	2.58	2.67	2.73	2.82	4.16	3.59	4.26	3.89	5.55	4.14	3.92
Cs	7.24	9.01	8.48	13.02	15.78	10.45	8.38	4.92	3.34	4.20	4.16	1.13	3.55	5.02
Ba	627	846	2319	30	71	294	648	358	897	357	232	121	343	278
La	19.42	18.61	13.89	4.57	4.89	4.82	4.76	7.57	7.24	7.68	6.59	10.25	8.16	7.61
Ce	42.08	39.63	30.86	11.20	11.53	11.69	11.60	18.67	17.14	18.52	16.27	23.57	19.84	17.95
Pr	5.38	4.86	4.02	1.52	1.65	1.59	1.61	2.62	2.22	2.63	2.24	3.20	2.78	2.49
Nd	21.99	19.64	16.39	7.06	7.80	7.42	7.61	12.19	11.11	12.08	10.58	14.03	12.28	11.33
Sm	4.61	4.05	3.64	1.97	2.37	2.52	2.12	3.34	2.86	3.03	2.81	3.29	3.23	2.95
Eu	1.43	1.44	1.40	0.82	0.85	0.87	0.84	1.22	1.29	1.30	1.21	1.34	1.30	1.25
Gd	4.65	4.29	4.17	2.94	3.26	2.93	2.96	3.85	3.98	3.98	3.64	4.12	4.10	3.76
Tb	0.72	0.69	0.66	0.55	0.59	0.52	0.54	0.70	0.65	0.68	0.60	0.70	0.64	0.67
Dy	4.55	4.27	4.26	3.36	3.72	3.66	3.54	4.25	3.79	4.17	3.72	4.21	4.31	4.09
Ho	0.95	0.84	0.87	0.81	0.83	0.78	0.81	0.89	0.85	0.87	0.84	0.88	0.85	0.90
Er	2.69	2.27	2.57	2.33	2.45	2.63	2.20	2.47	2.35	2.56	2.22	2.44	2.58	2.61
Tm	0.40	0.36	0.36	0.37	0.40	0.38	0.38	0.38	0.36	0.39	0.36	0.38	0.40	0.38
Yb	2.54	2.12	2.34	2.30	2.41	2.22	2.27	2.48	2.09	2.24	2.05	2.26	2.23	2.25
Lu	0.37	0.31	0.35	0.34	0.38	0.33	0.37	0.35	0.33	0.35	0.30	0.34	0.35	0.35
Hf	2.98	2.95	2.59	1.48	1.56	1.60	1.64	2.31	2.08	2.26	1.97	2.36	2.20	2.14
Ta	0.50	0.51	0.36	0.21	0.20	0.22	0.21	0.30	0.31	0.38	0.35	0.42	0.39	0.31
Pb	9.01	7.78	11.72	3.92	4.11	12.42	10.15	4.99	4.53	4.72	4.33	29.97	5.77	3.27
Th	4.20	4.00	3.32	1.15	1.02	0.80	0.85	0.95	0.71	0.99	0.74	1.46	0.97	0.80
U	0.95	0.84	0.57	0.35	0.30	0.19	0.17	0.17	0.13	0.17	0.15	0.24	0.15	0.21
$^{147}Sm/^{144}Nd$	0.127	0.125						0.166	0.156	0.152	0.161		0.159	
$^{87}Rb/^{86}Sr$	0.531	0.51						0.496	0.216	0.559	0.638		0.436	
$^{143}Nd/^{144}Nd \pm 2\sigma$	0.512597 ± 9	0.512632 ± 11						0.512820 ± 9	0.512816 ± 8	0.512830 ± 9	0.512797 ± 10		0.512797 ± 9	
$^{87}Sr/^{86}Sr \pm 2\sigma$	0.707838 ± 11	0.707805 ± 13						0.707401 ± 13	0.706703 ± 14	0.707596 ± 13	0.707249 ± 14		0.706402 ± 17	
$(^{87}Sr/^{86}Sr)i$	0.706176	0.706208						0.705849	0.706027	0.705848	0.705253		0.705036	
$\varepsilon_{Nd}(t)$	1.17	1.91						4.43	4.63	5.02	4.11		4.15	

Xiaodingxi and Manghuihe formations (Fig. 2) were studied with three of the sections, the Mianhuadi–Binglinghe, Pingcun and Jiukang sections, systematically sampled based on the lack of significant alteration and outcropping continuity of the samples. These three sections are the representative sections for the Xiaodingxi and Manghuihe volcanic sequences in Yunnan BGMR (1990, 1996). In this paper, a set of new geochronological, elemental and Sr–Nd–Pb isotopic data for forty typical samples are presented.

2. Geological background and petrography

The Lancangjiang tectonic zone is situated at the central part of the broader Nujiang–Lancangjiang–Jinshajiang tectonic belt, which is composed of the Changning–Menglian suture zone and Lancangjiang metamorphic and igneous zones and is regarded as the suture boundary of the eastern Paleotethys ocean. This zone separates the Simao Block in the east from the Baoshan Block in the west (Fig. 1a–b).

The Simao block is bounded by the Lancangjiang ophiolitic zone to the west and the Ailaoshan ophiolitic zone to the east (Fig. 1b). It is believed to have an affinity to the Yangtze Block (Liu, 1993; Zhong, 1998) or to represent the northern segment of the Indochina Block (e.g., Metcalfe, 1996; see Fig. 1a). In this block, the Proterozoic metamorphic basement is represented by the Damenglong and Chongshan complexes, which are mainly composed of metavolcanics, siliciclastics and marble (e.g., Zhong, 1998; Wang et al., 2006). The lower Paleozoic metasedimentary rocks show similar lithology to those of the Yangtze Block and are unconformably overlain by Devonian–Permian conglomerates and siliciclastic rocks (e.g., Yunnan BGMR, 1990; Zhong, 1998). The Baoshan Block is considered to be a component of the Sibumasu continental fragment with an affinity to Gondwana (Metcalfe, 1996; Zhong, 1998; Metcalfe, 2002). The basement for the Baoshan Block mainly comprises the Proterozoic granulite- and amphibolite-facies metamorphic rocks including the Ximeng, Langcang and Gaoligong groups (e.g. Yunnan BGMR, 1990, 1996; Zhong, 1998).

Our study area is located in the central part of the Lancangjiang tectonic zone (see locations of sections 1 to 6 in Fig. 1b). In the area, lower Paleozoic strata are absent. The upper Paleozoic (Devonian, Carboniferous, and Permian) and lower Triassic strata are composed of low-grade metamorphic clastics, volcanics and carbonate and are separated from the overlying upper Triassic–lower Jurassic Yiwanshui formation by an angular unconformity. The most remarkable geological feature of this area is the Lincang granite zone that extends 370 km and is up to 50 km wide along the Lancangjiang tectonic zone (Fig. 1b). This granite suite is a composite batholith composed of monzonitic biotite granite, K-feldspar granite and granodiorite, and has yielded ages of around 230 to 220 Ma (Helmcke, 1985; Liu et al., 1989; Peng et al., 2006).

The volcanic zone is distributed largely along the eastern margin of the granite zone from Yunxian to Jinghong (Fig. 1b). It strikes NNW or NNE over a distance of 300 km and is unconformably overlain by basal conglomerate of the Yiwanshui formation (Fig. 2). The volcanic zone extends northward to the Weixi–Deqin–Yushu areas, and southward to the Chiang Khong–Tak areas in northwest Thailand and further south to Peninsular Malaysia and the Indonesian islands of the Sunda Shelf (Fig. 1a–b; Sengor, 1979; Cobbing et al., 1992; Orberger et al., 1995; Metcalfe, 1996; Zhong, 1998; Tulyatid and Charusiri, 1999; Ueno and Hisada, 2001; Metcalfe, 2002).

The volcanic sequences in the area are traditionally grouped into the Triassic Manghua, Xiaodingxi and Manghuihe formations or their equivalents, with a combined thickness of more than 7400 m (Figs. 1a–b and 2; e.g., Yunnan BGMR, 1990, 1996; Mo et al., 1998; Zhong, 1998). The 924–1646 m thick Manghua Formation is located at the base and is composed of siltstone, high-K rhyolite and siliciclastic rocks with basaltic interlayers dispersed through the unit (e.g., Yunnan BGMR, 1990). Rhyolite from this formation yielded SHRIMP zircon U–Pb ages of 231–241 Ma (e.g., Peng et al., 2008; Fan et al., 2010). The Xiaodingxi and Manghuihe formations are located in the upper part of the volcanic sequence (see Fig. 2). They are abundantly distributed in the Yunxian, Jinggu, Lincang and Jinghong areas and are overlain by the Yiwanshui molasse. The Xiaodingxi Formation (2040 m thick) is composed of basaltic and andesitic rocks with a small amount of tuff and tuffaceous sandstone, siltstone, massive dacite and felsic breccia rocks (Fig. 2). The 3556 m thick Manghuihe Formation is underlain by the Xiaodingxi Formation, and contains basalt, basaltic andesite, andesite, rhyolitic lava, tuffaceous sandstone and pebbly sandstone (Fig. 2; Yunnan BGMR, 1990, 1996; Zhong, 1998). Our analyses are confined to basaltic rocks in the Xiaodingxi and Manghuihe volcanic sequences. The details of our investigated and sampled sections (the Mianhuadi–Binglinghe, Shantai, Nahan–Wenxiao, Dakunbo, Pingcun and Jiukang) are summarized in Fig. 2.

The analyzed rocks include basalt, basaltic andesite, andesite and trachyandesite. The basalt is mainly composed of 38–47% phenocrysts of clinopyroxene, plagioclase, and olivine or orthopyroxene, and 53–62% matrix of plagioclase, clinopyroxene, orthopyroxene, and amphibole. For the basaltic andesite, the most common mafic minerals are clinopyroxene and amphibole and felsic minerals are plagioclase with a small amount of biotite, quartz and Fe–Ti oxides. The andesite is commonly subaphyric to porphyritic, and is composed of plagioclase and clinopyroxene phenocrysts in a matrix of clinopyroxene, plagioclase and minor opaque oxide minerals. In the andesite, secondary chlorite is also commonly observed. The mineral compositions of the trachyandesite include amphibole, plagioclase, K-feldspar, quartz, biotite and minor titanite, apatite, zircon and Fe–Ti oxides. The sampling locations and lithological characteristics of the analytical samples are shown in Supplementary Table S1.

3. Analytical methods

Zircons were separated from rock samples using the conventional heavy liquid and magnetic techniques and purified by handpicking under a binocular microscope. The zircon grains were mounted in epoxy resin, polished, and coated with gold, and then examined for internal textures using the cathodoluminescence imaging (CL). U–Pb isotope analysis was conducted at the Beijing SHRIMP Ion Microprobe Center, the Chinese Academy of Geological Sciences. Detailed analytical procedures were similar to those described in Song et al. (2002) and Williams and Claesson (1987). The standard TEM zircons (age of 417 Ma) of RSES were used to determine the elemental discrimination that occurs during sputter ionization. The analytical results are listed in Table 1.

Major oxides were determined by X-ray fluorescence spectrometry at the Hubei Institute of Geology and Mineral Resource, the Chinese Ministry of Land and Resources. FeO content is analyzed by the wet chemical method. Trace element analyses were performed at the Institute of Geochemistry, Chinese Academy of Sciences (CAS) by an inductively coupled plasma mass spectrometry. About 100 mg samples are digested with 1 ml of HF and 0.5 ml HNO_3 in screw top PTFE-line stainless steel bombs at 190 °C for 12 h. The analytical precision is better than 5% for elements >10 ppm, less than 8% for those <10 ppm, and 10% for transition metals. The analytical results for the typical samples are presented in Table 2.

Analyses of Sr and Nd isotopic ratios were performed on the VG-354 mass spectrometer at the Institute of Geophysics and Geology, the CAS. The total procedure blanks were in the range of 200–500 pg for Sr and ≤50 pg for Nd. The mass fractionation corrections for isotopic ratios are based on $^{86}Sr/^{88}Sr = 0.1194$ and $^{146}Nd/^{144}Nd = 0.7219$. The measured $^{87}Sr/^{86}Sr$ ratios of the (NIST) SRM 987 standard and $^{143}Nd/^{144}Nd$ ratios of the La Jolla standard are 0.710265 ± 12 (2σ) and 0.511862 ± 10 (2σ), respectively. Pb was separated and purified by a conventional cation-exchange technique with diluted HBr as an eluant. Isotopic ratios were measured with the VG-354 mass spectrometer at the Institute of Geophysics and Geology, the CAS.

Repeated analyses of SRM 981 yielded the average values of $^{206}Pb/^{204}Pb = 16.942 \pm 4$ (2σ), $^{207}Pb/^{204}Pb = 15.498 \pm 4$ (2σ) and $^{208}Pb/^{204}Pb = 36.728 \pm 9$ (2σ).

4. Results

4.1. SHRIMP zircon U–Pb geochronology

Samples 02DX-103 and 02DX-124 were collected from the Xiaodingxi and Manghuihe sequences, respectively, along the Mianhuadi–Binglinghe section (Fig. 2). They are basaltic andesite and andesite, respectively, and their mineralogical compositions comprise clinopyroxene, plagioclase, amphibole, quartz, biotite and small amounts of magnetite, Fe–Ti oxides, euhedral zircon, titanite, apatite and chlorite.

Zircons separated from the two samples are mostly euhedral in morphology, and transparent and light brown in color. The CL images reveal oscillatory zoning with low to variable luminescence (Fig. 3a–b), indicative of igneous origin. Thirteen analytical spots for sample 02DX-103 gave a wide range of U (149–1284 ppm) and Th (94–501 ppm) concentrations, with Th/U ratios in the range from 0.15 to 0.71 (Table 1). Eleven analyses of these spots (with exception of spots G10 and G11) yielded a weighted mean $^{206}Pb/^{238}U$ age of 214 ± 7 Ma with MSWD = 1.4 (n = 11; Fig. 3c), which we interpreted as the crystallization age of the sample and the approximate age of the Xiaodingxi sequence. Seven spots were analyzed from sample 02DX-124 (fewer zircons were separated from this sample). Two analytical spots yielded older $^{206}Pb/^{238}U$ apparent ages (254 Ma and 310 Ma), which are interpreted as the ages of inherited zircons. The other five analyses gave Th = 98–1252 ppm and U = 462–1972 ppm with Th/U = 0.17–0.77, and yielded a weighted mean $^{206}Pb/^{238}U$ age of 210 ± 22 Ma with MSWD = 2.0 (Fig. 3d). This age is interpreted as the crystallization age of sample 02DX-124 and of the Manghuihe volcanic sequence. It is similar, within error, to that determined for the Xiaodingxi sequence.

4.2. Geochemical characteristics

4.2.1. Classification

The analyzed samples can be divided into two groups based on their MgO contents as well as Al_2O_3 contents and Zr/Nb ratios. As shown in Fig. 4a, Group 1 samples show MgO = 1.49–7.50%, Al_2O_3 = 15.95–18.39 wt.% and Zr/Nb = 9.4–15.3, whereas Group 2 samples have MgO of 8.08–11.74 wt.%, Al_2O_3 of 16.62–18.23 wt.% and Zr/Nb of 15.9–23.9. According to the classification of Kersting and Arculus (1994) and Morra et al. (1997), Group 1 samples plot into the low-Mg and high-Al basalt field, whereas Group 2 samples plot in the high-Mg and high-Al basalt field. On the SiO_2 vs K_2O+Na_2O diagram (Fig. 4b), Group 1 mainly plots into the alkaline basalt and basaltic trachyandesite fields, whereas Group 2 plots mainly in the trachybasalt field.

4.2.2. Elemental geochemistry

Group 1 samples display a wider range of SiO_2 (47.80–57.67 wt.%, volatile-free), FeOt (5.92–13.39 wt.%), Al_2O_3 (15.95–18.39 wt.%) and TiO_2 (0.87–2.37 wt.%) with an *mg*-number of 32–57, than Group 2 analyses. In Group 1 samples, MgO, FeOt, CaO, P_2O_5 and TiO_2 correlate negatively but Al_2O_3 positively with SiO_2, (Fig. 6a–f). Group 2 rocks display small variations in major oxide contents (Table 2), with SiO_2 = 47.50–50.76 wt.%, FeOt = 9.73–11.14 wt.%, Al_2O_3 = 16.62–18.23 wt.%, TiO_2 = 0.90–1.41 wt.% and *mg*-number = 58–68. A negative correlation is observed between CaO and SiO_2, but otherwise there is no clear correlation between other oxides and SiO_2 (Fig. 5a–f).

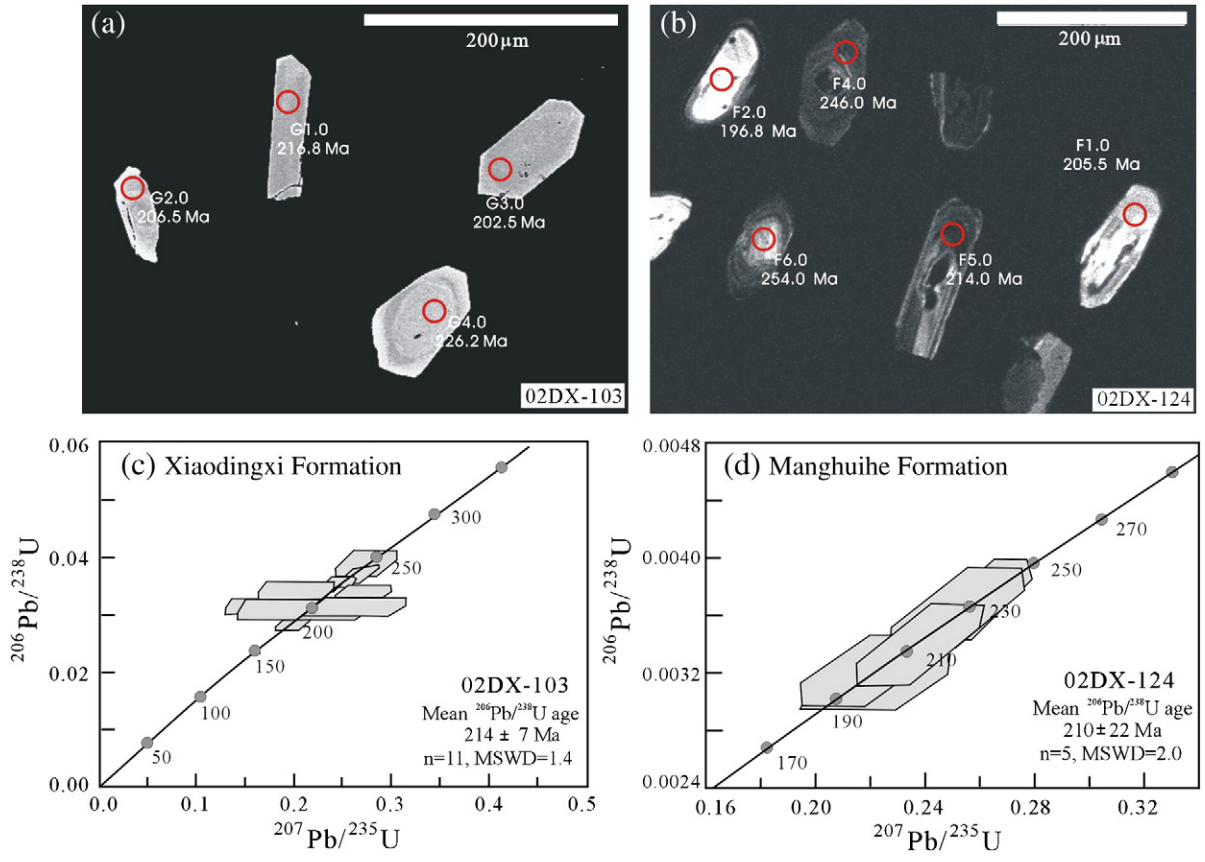

Fig. 3. (a–b) Cathodoluminescence (CL) images of representative zircon (a: sample 02DX-103 and b: 02DX-124) and (c–d) SHRIMP zircon U–Pb concordia diagrams (c: 02DX-103 and d: 02DX-124). Both samples are from the Xiaodingxi and Manghuihe volcanic sequences.

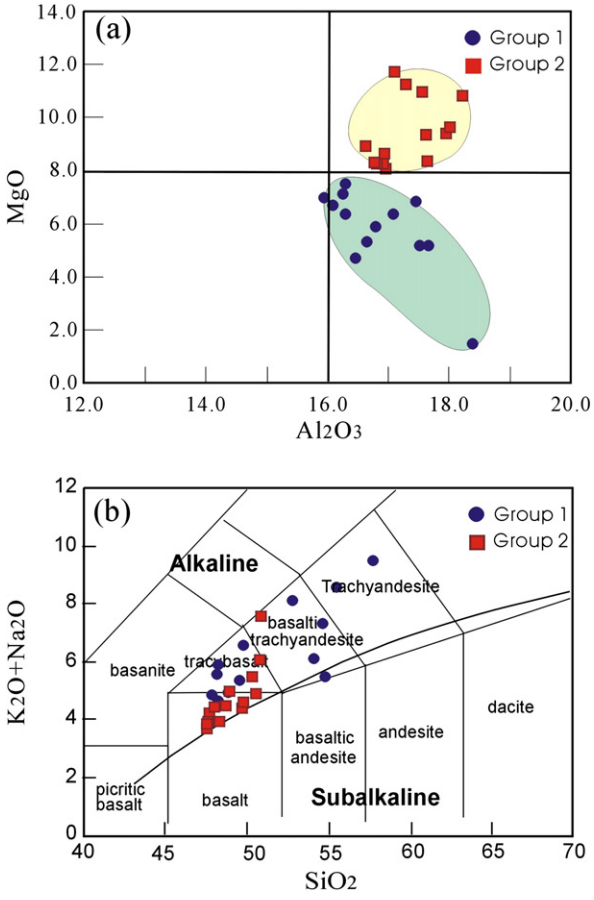

Fig. 4. (a) The classification diagram of Al_2O_3 and MgO and (b) SiO_2 vs $K_2O + Na_2O$ for the Xiaodingxi and Manghuihe volcanic rocks along the Lancangjiang tectonic zone.

Moreover, Group 2 exhibits higher Al_2O_3, MgO, Ni and Cr contents, but lower FeOt, TiO_2 and P_2O_5 contents at similar SiO_2 content than Group 1 (Table 2 and Fig. 5a–f).

Incompatible element compositions also show distinct features between Groups 1 and 2 (Table 2). Group 1 samples exhibit REE fractionation with (La/Yb)cn of 7.3–22.7 and (Gd/Yb)cn of 1.22–1.50, but Group 2 samples show the flat REE patterns with (La/Yb)cn of 1.47–2.11 and (Gd/Yb)cn of 0.92–1.34 (Table 2 and Fig. 6a–b). On multi-element diagrams (Fig. 6c–d), the Group 1 samples are characterized by marked negative Nb–Ta, Sr and Ti anomalies with Th/La = 0.09–0.35 and Nb/La = 0.26–0.66. Group 2 samples have Th/La = 0.11–0.25, Nb/La = 0.40–0.59, Ce/Pb = 4.2–18.0 and Nb/U = 4.01–38.7, and show significant negative Th–U and Nb–Ta anomalies, weak negative P–Ti anomalies and positive Sr anomalies. In comparison with Group 1, Group 2 shows lower LILE (large-ion lithophile elements) and LREE (light rare earth elements) contents in spite of similar HREE (heavy rare earth elements) contents.

4.2.3. Sr–Nd–Pb isotopic compositions

The Sr–Nd and Pb isotopic analytical results for the samples are presented in Tables 2 and 3, respectively. $^{87}Sr/^{86}Sr(t)$ ratios range from 0.705473 to 0.706972 for Group 1 and from 0.705253 to 0.706058 for Group 2. $\varepsilon_{Nd(t)}$ values vary from −1.47 to 0.75 for Group 1, contrasting with the range from 1.17 to 5.02 (majority in the range from 4.11 to 5.02) for Group 2 (Fig. 7a).

Pb isotopic compositions are shown in Fig. 7b–c. Group 1 samples plot above the Northern Hemisphere Reference Line (e.g., Hart, 1984, 1988), and $^{206}Pb/^{204}Pb = 18.394–8.995$, $^{207}Pb/^{204}Pb = 15.612–15.677$ and $^{208}Pb/^{204}Pb = 38.144–38.945$. Group 2 samples show Δ8/4 = 43.2–59.8 and Δ7/4 = 11.8–19.8. $^{207}Pb/^{204}Pb$ ratios are higher than those of the Indian Ocean and Atlantic–Pacific Ocean MORB at comparable $^{206}Pb/^{204}Pb$ ratios, indicative of more radiogenic ^{207}Pb content than ^{206}Pb. These Pb isotopic compositions are similar to those of the Middle Triassic Manghua volcanic rocks and global pelagic sediments (e.g., Ben Othman et al., 1989; Stolz et al., 1990; Vroon et al., 1993, 1995).

5. Discussion

5.1. Evaluation of alteration and crustal contamination en route

Loss on ignition (LOI) is an indicator of various degrees of low-temperature alteration after eruption. High LOI for samples in both groups (1.91–6.80 wt.%) suggests that these samples were likely affected by alteration. It is thus essential to evaluate whether or not these samples have undergone low-temperature alteration and crustal assimilation before discussing their mantle sources. For the Group 1 samples with less than 5.0 wt.% LOI, insignificant alteration is observed in their petrography (also see Supplementary Table S1). This is also consistently demonstrated by our data set (except for Rb, K and Ba), which shows similar patterns in multi-elemental diagrams and poor correlations between elemental and isotopic ratios and LOI (not shown). For Group 2 samples, there are insignificant correlations between LOI and Rb, Sr, Th, Sm, Nb, Nd, $Na_2O + K_2O$ and Sr–Nd–Pb isotopic ratios. This suggests that absolute abundances, ratios of incompatible elements (e.g., REE, Th, U, Nb, Ta, Zr, Hf, Y, and Ti) and isotopic ratios are slightly affected by alteration. Consequently in the discussion later we focus on samples with less than 5.0% of LOI.

For Group 1, almost all of the samples with less than 5.0 wt.% of LOI have similar Th/Ta ratios to primitive mantle (2.3) and high Nb/U ratios close to MORB and OIB. These samples have higher TiO_2 contents than Group 2 samples and relatively constant $^{87}Sr/^{86}Sr(t)$ and $\varepsilon_{Nd}(t)$ values irrespective of the SiO_2 content (not shown). These features, together with the lack of correlation between MgO and Ce/Pb and Nb/U, and the similarity of immobile incompatible element patterns, are clearly contrary to what would be expected for the rocks affected by crustal contamination.

The Group 2 samples have high MgO (more than 8.0 wt.%), Cr (154–293 ppm) and Ni (74–202 ppm) contents and low Th and U contents, although the positive and negative correlations of SiO_2 with $^{87}Sr/^{86}Sr(t)$ and $\varepsilon_{Nd}(t)$ are observed, respectively (not shown). The Th/Ta ratios range from 2.14 to 9.28 (Table 2). These features argue against any crustal contamination during magma transport. This is also supported by relatively constant Nb/La and Nb/U ratios irrespective of the MgO content. The observation of few inherited zircon in the two dated samples is also evidence for little or no crustal contamination.

5.2. Petrogenesis of Group 1 samples

5.2.1. Fractionation of primitive high-Mg and low-Al magma

The Group 1 samples are high-Al basalt and basaltic andesite. Four scenarios can be proposed for the formation of the high-Al samples: (1) high degree partial melting of the subducted oceanic crust (Marsh, 1976; Baker and Eggler, 1983; Brophy and Marsh, 1986; Myers, 1988; Myers and Johnston, 1996); (2) extensive interaction of ascending melts with refractory mantle (Kelemen, 1995; Rivalenti et al., 1998); (3) plagioclase accumulation in low-MgO magmas (Gust and Perfit, 1987; Brophy, 1988; Crawford et al., 1989; Fournelle and Marsh, 1991); and (4) olivine and clinopyroxene fractionation of the primitive high MgO and low Al_2O_3 melts (e.g., Perfit et al., 1980; Kersting and Arculus, 1994; Lytwyn et al., 2001; Schiano et al., 2004). We assess each of these scenarios later.

Partial melting of the subducted oceanic crust typically generates adakitic magma with high Si, Al, and Sr (>400 ppm) and Sr/Y (>20) and low Y (<18 ppm) and Yb (<1.9). However, the presence of late Triassic adakites in the study area has not been reported. In addition,

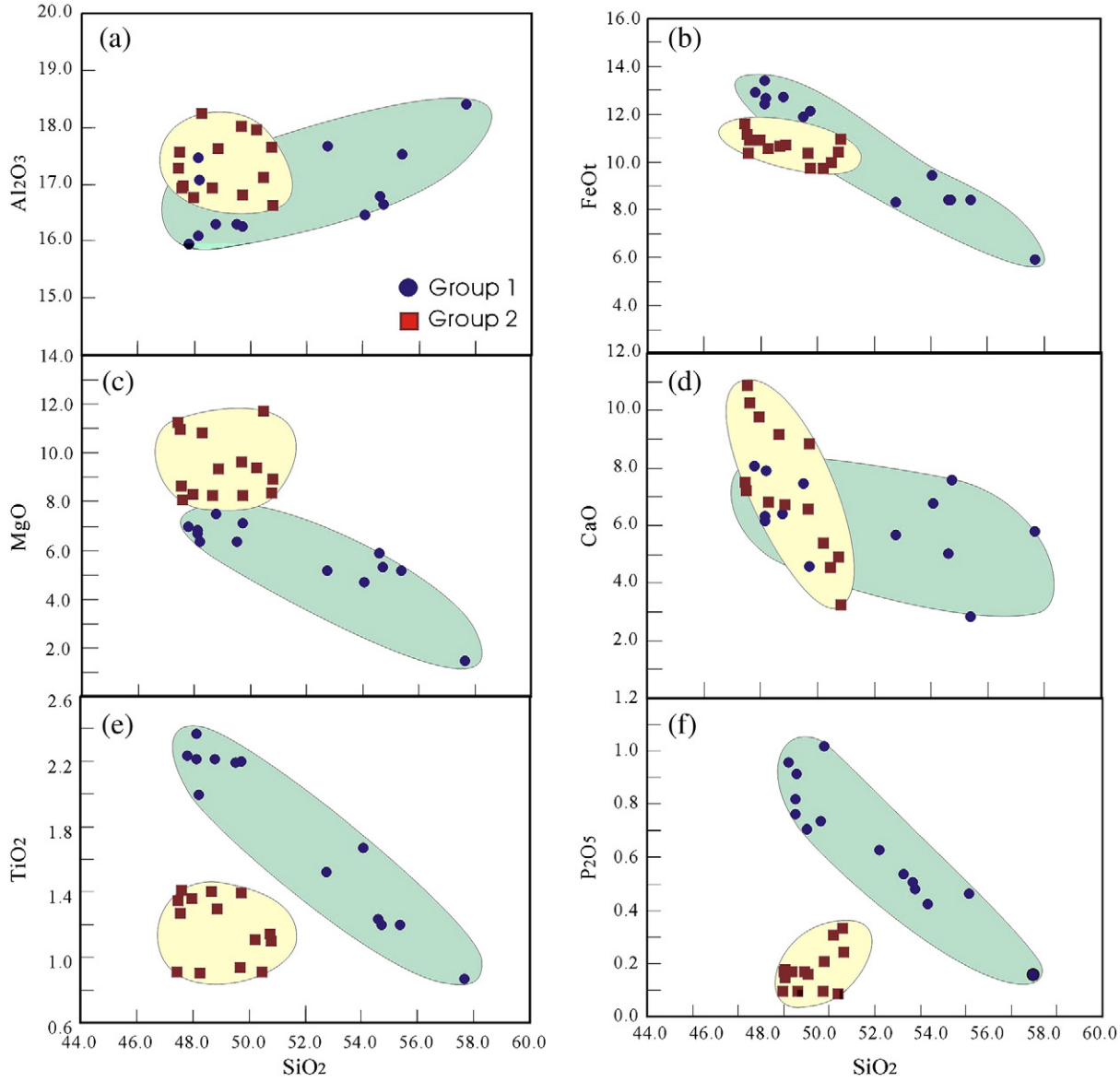

Fig. 5. Plots of SiO_2 vs (a) Al_2O_3, (b) FeOt, (c) MgO, (d) CaO, (e) TiO_2 and (f) P_2O_5 for Groups 1 and 2 samples along the Lancangjiang tectonic zone.

rocks generated by the melts of the young oceanic crust would show strongly fractionated LREE/HREE ratios with $(La/Yb)_{cn}$ >20 and depleted Sr–Nd isotopic composition ($^{87}Sr/^{86}Sr$ <0.705 and $\varepsilon_{Nd}(t)$ >4, Brophy and Marsh, 1986; Johnston, 1986; Myers, 1988; Defant and Drummond, 1990). Such features are not observed in the Group 1 samples. In addition, regional relations suggest that subduction within the main Paleotethys ocean, along the Lancangjiang suture, occurred during Permian (e.g., Zhong, 1998), which argues against the subduction of the young oceanic crust in the latest Triassic. Therefore, scenario (1) involving melting of subducted oceanic crust is unlikely for the petrogenesis of the Group 1 rocks.

The interaction of ascending melts with the refractory mantle can lead to high-Al basaltic magma, as suggested by Kelemen (1995). However, the magma derived from the interaction between melt and peridotite will usually be characterized by higher *mg*-number and Cr and Ni contents than those in normal peridotite-derived melt. Such characteristics are inconsistent with those of Group 1 samples which have *mg*-numbers of 32–57, Cr of 10–168 ppm and Ni of 4–60 ppm. Therefore, scenario (2) involving interaction of ascending melts with the mantle is also not likely in the petrogenesis of the samples.

Plagioclase accumulation in low-MgO magma is regarded as an alternative for generating high-Al basaltic rocks. However, plagioclase accumulation would result in increasing Sr and CaO and positive Sr and Eu anomalies in the magma, which contrasts with the geochemical characteristics observed for Group 1. In addition, evidence for plagioclase accumulation has not been observed in thin sections. Hence, plagioclase accumulation is unlikely as a possible mechanism for generating the Group 1 rocks.

Olivine and clinopyroxene fractionation in parental melts is the most likely explanation for the formation of the Group 1 high-Al rocks. This interpretation is based on the following features observed in Group 1 samples: (1) low *mg*-number (0.48–0.57) and low-MgO (mostly <8.0 wt.%), Cr (10–174 ppm) and Ni contents (4–61 ppm) (Table 2); (2) negative correlations of SiO_2 with MgO, CaO, and FeO (Fig. 5a–d); (3) positive correlations between MgO and CaO/Al_2O_3, Cr and Ni (Fig. 8a and c); (4) the decrease of V and Ni with the decrease in Cr, suggesting hornblende fractionation to some degree (Fig. 10b and d); (5) negative Sr and P–Ti anomalies, relatively low Eu/Eu^* values (Fig. 6a and c), and positive correlations between MgO and P_2O_5 and TiO_2 (Fig. 6h and i). In addition, the correlations in Fig. 6a–f

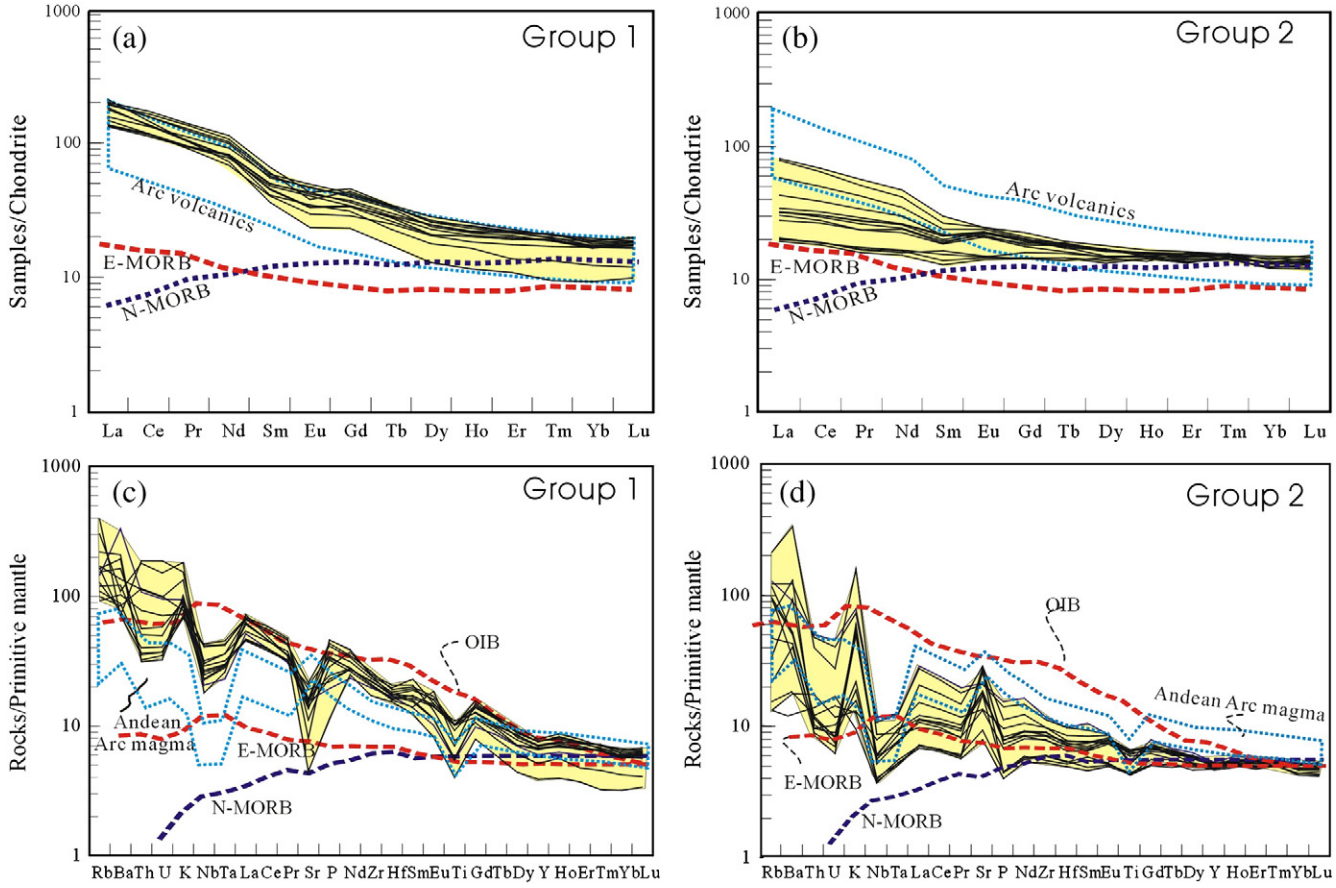

Fig. 6. (a–b) The patterns of the chondrite normalized rare earth elements and (c–d) primitive mantle-normalized spidergram for Groups 1 and 2 samples along the Lancangjiang tectonic zone, respectively. Chondrite- and primitive mantle-normalized values are from Taylor and McLennan (1985), and Sun and McDonough (1989), respectively. Dashed circle notes the field of arc-volcanic rocks/Andean arc magma (Pearce et al., 1995). Data for OIB, N-MORB, E-MORB and arc-volcanic rocks/Andean Arc magma are after Sun and McDonough (1989) and Shinjo et al. (1999).

also indicate that the primitive magma of Group 1 is characterized by high MgO, FeOt, TiO_2 and P_2O_5 and low Al_2O_3. The experimental studies also support the consideration that the high-Al samples can be generated by the olivine and clinopyroxene fractionation of parental melts (e.g., Perfit et al., 1980; Kersting and Arculus, 1994; Lytwyn et al., 2001; Schiano et al., 2004).

5.2.2. A metasomatized source modified by the recycled sediments

The question remains as to the source of the parental magma for Group 1. These samples show enrichment in LILEs and depletion in HFSEs with pronounced negative Nb–Ta anomalies (Fig. 6c). Zr/Nb ratios range from 9.3 to 15.3 and Nb/La from 0.26 to 0.66, similar to those of typical arc magmas (Brophy and Marsh, 1986; Oźerov, 2000;

Table 3
Pb isotopic compositions of typical samples from the Xiaodingxi and Manghuihe formations.

Sample		$^{238}U/^{204}Pb$	$^{232}Th/^{204}Pb$	$^{235}U/^{204}Pb$	$^{206}Pb/^{204}Pb$	$^{207}Pb/^{204}Pb$	$^{208}Pb/^{204}Pb$	$(^{206}Pb/^{204}Pb)i$	$(^{207}Pb/^{204}Pb)i$	$(^{208}Pb/^{204}Pb)i$	Δ7/4	Δ8/4
02DX-12	Group 1	10.691	50.998	0.078	18.849	15.631	38.89	18.478	15.612	38.332	11.8	36.5
02DX-33		14.051	67.785	0.102	19.094	15.692	39.298	18.606	15.667	38.556	15.9	43.4
02DX-103		21.091	96.822	0.153	19.135	15.649	39.204	18.403	15.612	38.144	12.6	26.8
02DX-105		28.959	75.487	0.210	19.399	15.693	39.024	18.394	15.642	38.198	15.7	33.3
02DX-108		4.124	16.830	0.030	18.879	15.661	38.858	18.736	15.654	38.674	13.2	39.5
02DX-109		5.445	22.638	0.039	19.184	15.687	39.193	18.995	15.677	38.945	12.7	35.3
02DX-116		3.615	14.612	0.026	18.821	15.648	38.693	18.695	15.642	38.533	12.4	30.3
02DX-117		3.598	14.347	0.026	18.956	15.676	38.855	18.831	15.670	38.698	13.7	30.4
02DX-120		2.792	10.830	0.020	18.788	15.626	38.656	18.691	15.621	38.537	10.4	31.3
02DX-121		4.952	20.905	0.036	18.764	15.634	38.684	18.592	15.625	38.455	11.9	35.0
02DX-7	Group 2	6.782	31.057	0.049	18.861	15.708	39.076	18.626	15.696	38.736	18.6	59.1
02DX-8		6.890	34.106	0.050	18.777	15.631	38.844	18.538	15.619	38.471	11.8	43.2
02DX-21		2.227	12.588	0.016	18.581	15.635	38.632	18.504	15.631	38.494	13.4	49.6
02DX-22		1.809	10.353	0.013	18.619	15.692	38.773	18.556	15.689	38.660	18.6	59.8
02DX-24		2.314	13.963	0.017	18.673	15.709	38.855	18.593	15.705	38.702	19.8	59.7
02DX-27		1.699	11.022	0.012	18.456	15.629	38.538	18.397	15.626	38.417	14.1	54.8

$\lambda_{U238} = 1.55125*10^{-10}$/year, $\lambda_{U235} = 9.848*10^{-10}$/year, $\lambda_{Th232} = 4.9475*10^{-11}$/year. Initial Pb isotopic ratios were calculated using the measured whole-rock Pb isotopic compositions, whole-rock U, Th and Pb contents (ICP-MS) by assuming 215 Ma for these samples. $\Delta 7/4 = ((^{207}Pb/^{204}Pb)_i - (^{207}Pb/^{204}Pb)_{NHRL})*100$; $\Delta 8/4 = ((^{208}Pb/^{204}Pb)_i - (^{208}Pb/^{204}Pb)_{NHRL})*100$; $(^{207}Pb/^{204}Pb)_{NHRL} = 0.1084*(^{206}Pb/^{204}Pb)_i + 13.491$ (Hart, 1984); $(^{208}Pb/^{204}Pb)_{NHRL} = 1.209*(^{206}Pb/^{204}Pb)_i + 15.627$ (Hart, 1984).

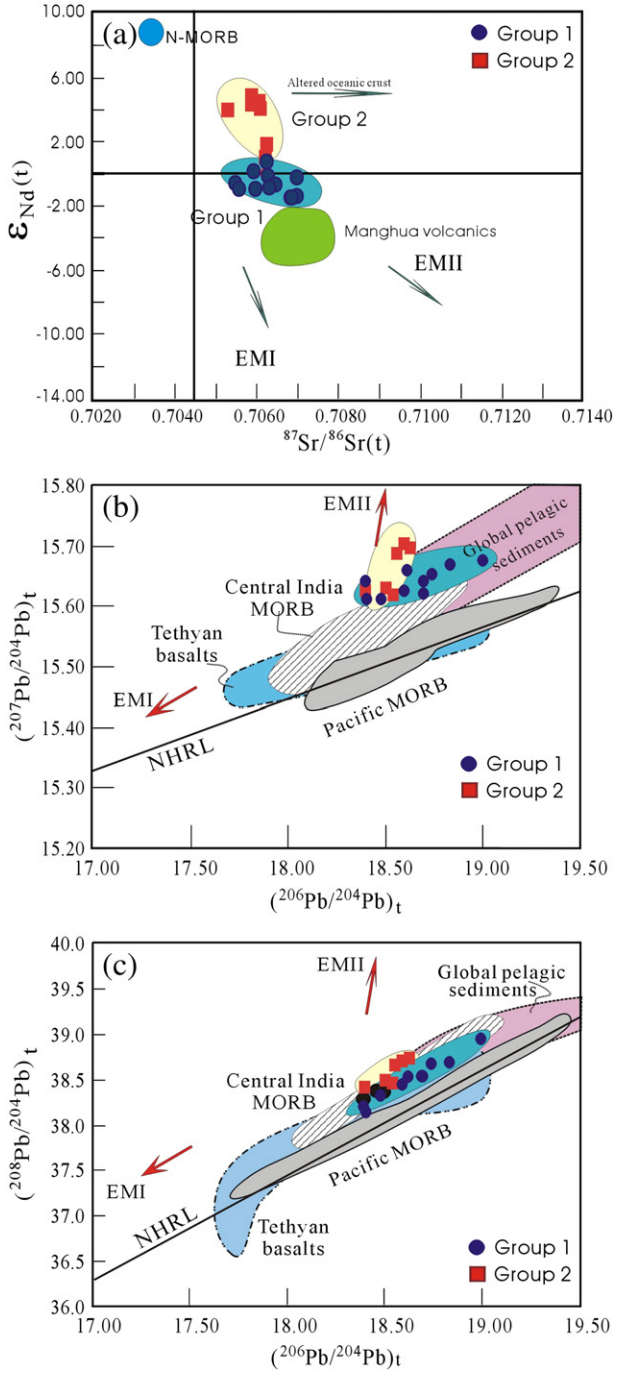

Fig. 7. (a) Plot of initial $^{87}Sr/^{86}Sr(t)$ vs $\varepsilon_{Nd}(t)$ (t = 210 Ma) for Groups 1 and 2 samples along the Lancangjiang tectonic zone. These samples are plotted along the mantle array between the depleted and enriched lithospheric components (Hart, 1984, 1988; Hawkesworth et al., 1984; Rehkämper and Hofmann, 1997). (b) and (c) Initial $^{207}Pb/^{204}Pb$ (a), $^{208}Pb/^{204}Pb$ (b) vs $^{206}Pb/^{204}Pb$ diagrams for Groups 1 and 2 samples. The field of EM1 and EM2, and the Northern Hemisphere Reference Line (NHRL) are from Hart (1984, 1988). The data for the central Indian Ocean MORB, Pacific MORB, Tethyan Basalts and global pelagic sediments are dominantly from Ben Othman et al. (1989) and Vroon et al. (1993, 1995).

Luhr and Haldar, 2006). These characteristics, together with the (Ta/La)n ratios of 0.45–0.70 and (Hf/Sm)n ratios of 0.90–1.25, suggest the involvement of a "crustal" component in the source. This is also reflected by the Sr–Nd–Pb isotopic compositions with a trend towards the crustal/sedimentary component along the mantle array (Fig. 7a–c). An uncertainty still remains as to whether such "crustal" signatures originated from dehydrated fluids/melts from subducted slab/sediments. Sr/La ratios for Group 1 samples have narrow variation irrespective of La/Yb ratios (Fig. 9a). The Th/Yb ratios of these samples show a sharp change in spite of small variations in Ba/La ratios, favoring the scenario for the involvement of recycled sediments (Fig. 9b).

The remarkable increase of Th/La ratios with increasing Ce/Pb argues for an origin involving metasomatized source modified by subducted sediment (Fig. 9c), potentially via source contamination during the subduction process. This is also supported by the rapid changes of the Nb/Y and Nb/Zr ratios with Ba/Y and Th/Zr, and the pronounced decrease in Nb/U with decreasing $\varepsilon_{Nd}(t)$ values. Other evidence supporting the involvement of subducted sediments in the source for Group 1 samples includes: (1) $^{87}Sr/^{86}Sr$ ratios of 0.705473–0.706972, (2) Pb isotopic compositions similar to the average values for global pelagic sediments, and (3) higher Th/Ce, Nb/Zr and Th/Nb ratios and lower Pb/Nd ratios than those of MORB.

Fig. 9d–f shows a negative correlation between Sr and Pb isotopic compositions and a positive correlation between $\varepsilon_{Nd}(t)$ vs $^{206}Pb/^{208}Pb$ and Nb/La for Group 1 samples. These patterns most likely suggest a binary mixing source for the Group 1 samples, as documented by Zou et al. (2000). One component of the binary end-members is characterized by high $^{87}Sr/^{86}Sr$ (>0.7070), low $^{206}Pb/^{204}Pb$ (<18.40) and Nb/La (<0.3), similar to the estimates for crustal sediments. The other is a high $^{206}Pb/^{204}Pb$ (>19.0) and Nb/La (>0.8) and low $^{87}Sr/^{86}Sr$ (<0.7040) component, with similarities to an enriched lithospheric component. A similar mixing trend is also observed in the plots of the incompatible element ratios (not shown). Available data show that Carboniferous mantle source in the study area is compositionally similar to the present-day Indian MORB (Michard et al., 1986; Rehkämper and Hofmann, 1997; Zhong, 1998). To define the contribution of pelagic sediments in the source for Group 1, a mixing calculation was performed based on Nd–Pb isotopic compositions with the Indian MORB component and pelagic sediment as the potential end-members, respectively (Ben Othman et al., 1989; Vroon et al., 1993, 1995). The results shown in Fig. 10a indicate that the involvement of 5–10% pelagic sediment into a MORB source can explain the isotopic compositions of the Group 1 samples.

5.3. Petrogenesis of Group 2 samples

5.3.1. Partial melting of a plagioclase-rich, garnet-free source

The Group 2 samples are predominantly high-Al and high-Mg basaltic rocks. They show rapidly decreasing Cr and Ni, and slightly decreasing FeOt with magma evolution (Figs. 5b and 8a and c), indicative of various degrees of olivine and clinopyroxene fractionation for the parental magmas. Such fractionation is also supported by the clear correlations shown on the plots of Cr vs Ni and V (Fig. 8b and d) and Sr vs Ba (not shown). A question remains as to whether Group 2 magmas are the fractionated product of high MgO and low Al_2O_3 primitive melts, as in the case of Group 1 (e.g., Lytwyn et al., 2001; Schiano et al., 2004).

As illustrated in Fig. 5a–f, the Group 2 samples have rather narrow ranges of SiO_2 variations and show only minor changes of other oxides (exception for CaO) with increasing SiO_2. They have *mg*-numbers of 58–68, MgO of 8.08–11.74 wt.%, Cr of 154–293 and Ni of 74–202, close to those of the primitive magma. The examination of the data for individual samples is particularly useful. (1) Al_2O_3 for sample 02DX-25 reaches 16.93 wt.% although SiO_2 is as low as 47.56 wt.%, and *mg*-number (61) and MgO (8.62 wt. %) are both relatively high. (2) For sample 02DX-34, Al_2O_3 = 17.56 wt.% when SiO_2 = 47.50 wt.%, *mg*-number = 65 and MgO = 10.95 wt.%. These characteristics, together with the correlations shown in the Harker diagrams (Fig. 5a–f), suggest that parental magma for Group 2 should be characterized by high Al_2O_3 (>16.50%) and MgO (>8.0%) and relatively low FeOt, TiO_2 and P_2O_5. The high-Al and high-Mg features of Group 2 samples might

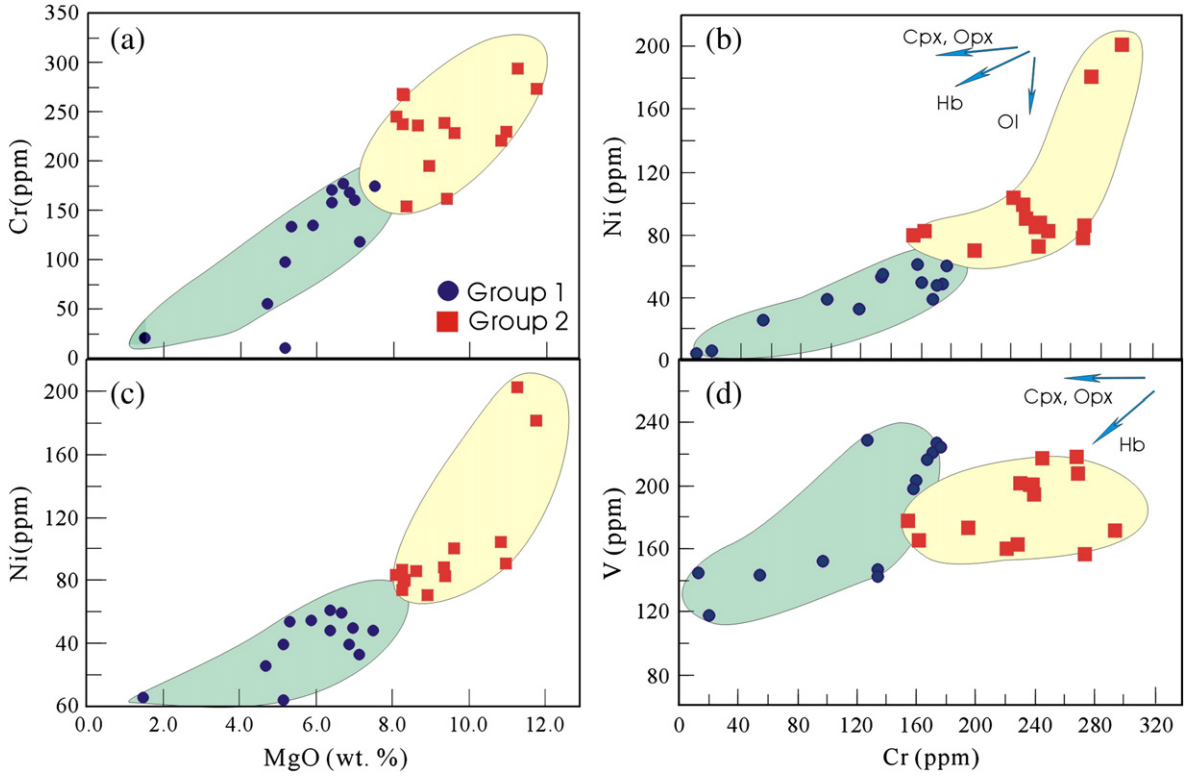

Fig. 8. (a) MgO vs Cr, (b) Cr vs Ni, (c) MgO vs Ni and (d) Cr and V for Groups 1 and 2 samples along the Lancangjiang tectonic zone.

be mainly related to the partial melting of a heterogeneous source, rather than to fractionation in primitive low-Al magma.

Low La/Yb ratios typically reflect a melting regime dominated by relatively large degree of partial melts or spinel as the main residual phase, whereas high La/Yb ratios are indicative of smaller melting fractions and garnet control (e.g., Deniel, 1998). Group 2 has low P_2O_5/Al_2O_3, La/Yb, Sm/Yb and Ce/Y and near-chondrite (Gd/Yb)n ratios, suggestive of melting conditions under low pressure or high melting proportion (e.g., Deniel, 1998; Espinoza et al., 2005). The garnet-free refractory source is also evidenced by the poorly increasing (Sm/Yb)n with increasing (La/Sm)n. Almost all of the Group 2 samples show insignificant P–Ti and Eu anomalies (Fig. 7a and c), arguing against significant plagioclase fractionation during magma evolution. As a result, the positive Sr anomaly displayed by Group 2 samples was most likely inherited from a plagioclase-rich source (Rehkämper and Hofmann, 1997; Sobolev et al., 2000). The presence of accumulated plagioclase in the source can explain the Th–U depletion of the Group 2 samples (e.g., Zimmer et al., 1995; Sobolev et al., 2000). Therefore, we propose that Group 2 magmas are formed by partial melting of a heterogeneous, plagioclase-rich, garnet-free source followed by fractionation of olivine and pyroxene. This is consistent with experimental results showing that plagioclase-rich spinel lherzolite can be partially melted to generate high-Mg and -Al basaltic magma with high Sr contents (Fujii and Scarfe, 1985; Falloon and Green, 1987; Bartels et al., 1991).

5.3.2. A hybridized source of N-MORB

A remaining question concerning the petrogenesis of Group 2 is what components were involved in the heterogeneous source for these samples. The Group 2 samples exhibit enrichment in LILEs, depletion in HFSE and positive Pb anomalies, and have a similar pattern as the Andean arc volcanics for strongly incompatible elements (Fig. 6d). High Sr/La and Ba/La and low Th/Yb and Ce/Pb ratios strongly suggest that crustal component plays an important role in the petrogenesis of Group 2. However, a number of previous studies (e.g., Zhang et al., 1996; Ma et al., 1998; Zhang et al., 2002) reported that the Simao basement has an affinity to the Yangtze Block that is characterized by low Sr/La and relatively low radiogenic Pb isotopic ratios (e.g., Zhang et al., 1996, 2002). Therefore, the high Sr/La ratios and high Pb isotopic compositions of Group 2 cannot be attributed to the involvement of recycled crustal sediments from the Simao Block, but are rather are most likely related to subduction-derived fluids. The trends in Fig. 9a–c are also consistent with an increasing hydrous metasomatism related to subduction-derived fluids.

These samples also show high $\varepsilon_{Nd}(t)$ values of $+4.11$–$+5.02$ (except for samples 02DX-07 and -08) and hence have an affinity to a MORB source. The flat pattern of moderately incompatible elements also indicates the MORB signatures of the samples (Fig. 6d). The (Ta/La)n and (Hf/Sm)n ratios are close to those of N-MORB, suggesting the involvement of a N-MORB component in the generation of Group 2. As illustrated in Fig. 9d–f, the Group 2 samples plot along an array distinct from that of the Group 1 rocks. The correlations in the Sr–Nd–Pb diagrams (Fig. 9d–f) also most likely suggest a binary mixing origin for Group 2. One end-member might be a component with Nb/La of >0.7, $^{206}Pb/^{204}Pb$ of <18.40, $\varepsilon_{Nd}(t)$ of >7.0 and $^{87}Sr/^{86}Sr$ of <0.7050, probably equivalent to those of MORB. The same conclusion can be reached by examining the plots of incompatible elemental vs isotopic ratios (Fig. 9f) and incompatible elemental ratios (e.g., Nb/U vs Th/La). The other end-member is apparently related to a metasomatized lithospheric mantle.

To quantify the contributions of the two end-members, a modeling calculation was performed using the average Group 1 source and N-MORB as two potential components. When assuming $\varepsilon_{Nd}(t) = +9$ and -1.0 for the N-MORB and average Group 1 source as end-members in Fig. 9e–f (Hawkesworth et al., 1984), the involvement of 15–20% N-MORB can explain the Nd isotopic variations for Group 2. The modeling results of incompatible element ratios (Fig. 10b) show that the addition of about 18% N-MORB component into a subduction-modified Group 1 source can explain the variations of the incompatible elements for the Group 2 rocks. The subducted oceanic

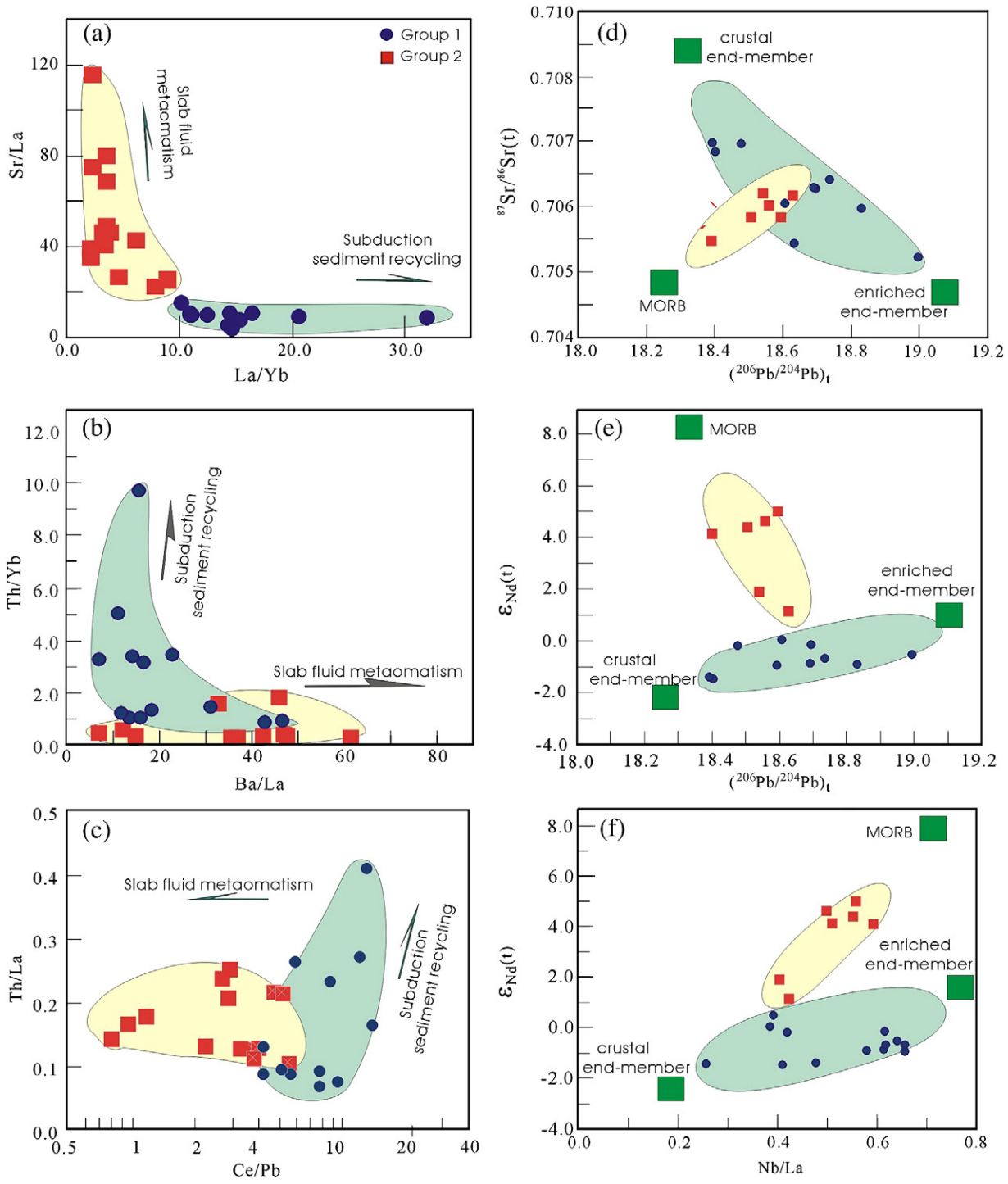

Fig. 9. Plots of La/Yb vs Sr/La (a), Ba/La vs Th/Yb (b), and Ce/Pb vs Th/La (c) $^{206}Pb/^{204}Pb$ vs (d) $\varepsilon_{Nd}(t)$ and (e) $^{87}Sr/^{86}Sr$ and (f) Nb/La vs $\varepsilon_{Nd}(t)$ for Groups 1 and 2 samples along the Lancangjiang tectonic zone. The subduction sediment recycling results into the significant increasing La/Yb and Th/Yb but the slab fluid metasomatism into the sharply increasing Sr/La and Ba/La. Group 1 samples are plotted along the binary mixing between the crustal and enriched lithospheric end-members and Group 2 samples are clearly derived from a hybridized source with the involvement of MORB component.

crust and the upwelling asthenospheric component are the possible candidates for the MORB end-member. The young oceanic crust is generally transformed to eclogite-facies during subduction (e.g., Cooke and O'Brien, 2001), and was recycled into the mantle as eclogitic layers or pods to hybridize with refractory peridotite (Hemond et al., 1994). However, the subduction of the Paleotethys oceanic crust along the Lancangjiang suture occurred in the earliest Permian, arguing against the subduction of the young oceanic crust and phase-transformation from the oceanic basalt into eclogite during the latest Triassic (e.g., Zhong, 1998; Mo et al., 1998; Peng et al., 2008; Hennig et al., 2009). Experimental studies (e.g., Rapp et al., 1991) indicated that the partial melting of eclogite would generate magma with high SiO_2 (>56 wt.%), Al_2O_3 and TiO_2. As such, rocks derived from a hybridized source with the involvement of the recycled oceanic crust should have higher SiO_2 Al_2O_3 and TiO_2 than those of Group 1. This contrasts with the observation that the Group 2 samples have lower SiO_2 and TiO_2 than the Group 1 rocks at comparable Al_2O_3. As described above, Group 2 magma originated

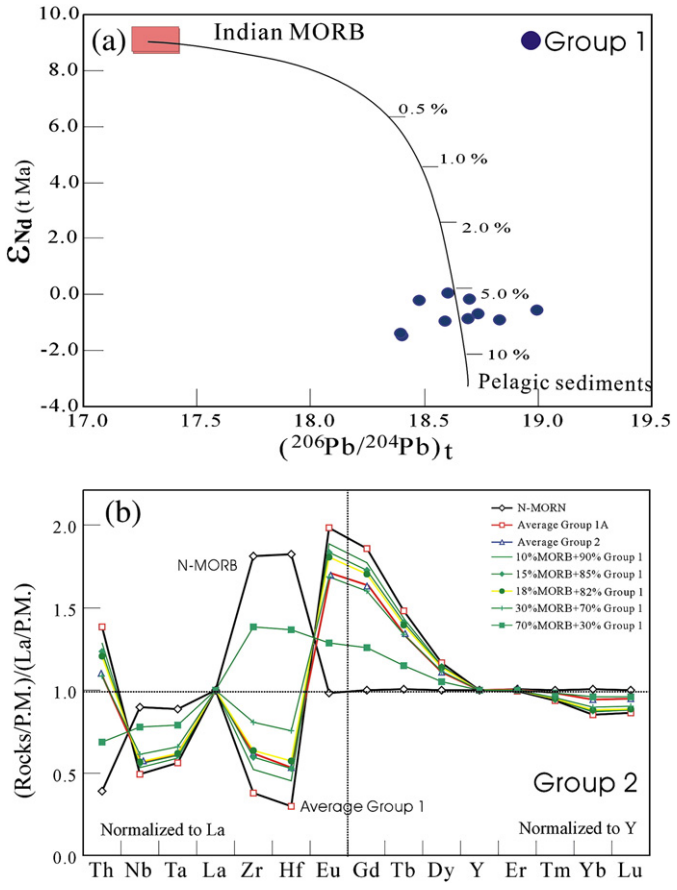

Fig. 10. Modeling of (a) $^{206}Pb/^{204}Pb$ and $\varepsilon_{Nd}(t)$ for the Group 1 samples, and (b) the incompatible element ratios for Group 2 using N-MORB and average Group 1 as two potential components. Strongly (from Th to Eu) and moderately (from Gd to Lu) incompatible elements are normalized to La and Y, respectively. Addition of ca. 18% N-MORB component into the lithospheric mantle can account for the variations of the incompatible element ratios for the Group 2 magma.

from a plagioclase-rich and garnet-free source. Therefore, an alternative for the MORB end-member is represented by the upwelling asthenospheric mantle (e.g., Shimoda et al., 1998). In summary, the Group 2 primary magma originated from a hybridized source composed of 15–20% upwelling asthenospheric mantle and 80–85% subduction fluid-metasomatized component.

5.4. Tectonic implications

The Lancangjiang tectonic zone in southwest China separates the Simao–Indochina from the Baoshan–Sibumasu blocks (e.g., Metcalfe, 1996; Zhong, 1998; Metcalfe, 2002). Features related to the Paleotethys that are preserved along the zone include: (1) abundant Devonian and Permian mélange, ophiolite suite, oceanic and oceanic-island basalts, shallow-marine carbonates and deep-sea sedimentary rocks (e.g., Zhong, 1998 and references therein); (2) high-pressure blueschist at Shuangjiang, which (glaucophane) yielded a $^{40}Ar/^{39}Ar$ plateau age of 279 Ma (e.g., Zhong, 1998); (3) magmatic arc igneous zone (Fig. 1b) that extends from west Jinghong to Lincang then to Yunxian (Zhong, 1998; Mo et al., 1998), which was dated at 284–249 Ma (Yu et al., 2003; Peng et al., 2008; Hennig et al., 2009); (4) the Nanlianshan volcano–plutonic complex with MORB-like geochemical affinity, which yielded a U–Pb zircon age of 292 ± 1 Ma, and the associated granodiorite dated by U–Pb zircon at 284–282 Ma (Hennig et al., 2009); and (5) the Shuangjiang ophiolite and Banpo Alaskan-type gabbro (south of Lincang, see Fig. 1b), which yielded SHRIMP zircon U–Pb ages of 288–264 Ma (Jian et al., 2004, 2009). In addition, along the Jinshajiang–Ailaoshan and Song Ma tectonic zone (north of Lancangjiang), there are abundant late Paleozoic mafic–ultramafic complexes (e.g., Shuanggou, Susong and Zhiyong) and plagiogranite (e.g., Xuetui and Liangjiuding) as well as Permian (285–267 Ma) mafic rocks (e.g., the Baimaxueshan and Gicha gabbros, Yaxuanqiao and Wusu basaltic rocks) showing back-arc basin geochemical affinities (Fig. 1; Jian et al., 1998, 2003, 2004, 2008, 2009; Fan et al., 2010). The Lancangjiang tectonic zone is correlated to the south with the Inthanon and Sukhothai zones in Thailand that are treated as the Paleotethys suture zone and Permian island-arc zone on the western margin of the Indochina Block, respectively. Nan–Sra Kaeo ophiolitic mélanges that lie at the eastern end of the Sukhothai zone are regarded as a disrupted back-arc basin succession (Sone and Metcalfe, 2008 and reference therein). Fan et al. (2010) recently reported geochronological and geochemical data from the Wusu and Yaxuanqiao basaltic rocks along the Ailaoshan tectonic zone. This data suggested the development of a Permian arc-back-arc basin along the Ailaoshan tectonic zone in response to the northward subduction of the main Paleotethys ocean. Therefore, we propose herein a similar evolution for the Paleotethys in southwest China. Specifically, the Changning–Menglian and Lancangjiang metamorphic and igneous zones correspond to the Inthanon and Sukhothai zones, respectively, and together constituted the Lancangjiang tectonic zone. The Nan–Sra Kaeo ophiolitic mélanges might correlate with Ailaoshan back-arc tectonic zone.

The subsequent collision of the Simao block with the Baoshan block along the Lancangjiang tectonic zone can be constrained to the middle Triassic based on the geological and geochemical characteristics of the syn-collisional representative involving the Manghuai volcanic sequence and their equivalents (e.g., Yunnan BGMR, 1990; Zhong, 1998; Mo et al., 1998; Shen et al., 2002; Peng et al., 2006). The Manghuai intermediate–felsic volcanic rocks unconformably overlie pre-Triassic strata and have a paraconformable contact with the overlying Xiaodingxi and Manghuihe formations. The middle Triassic Lincang granitic batholith (243–227 Ma) has been interpreted as the intrusive equivalent of the Manghuai volcanic sequence (238–231 Ma; Zhong, 1998; Hou et al., 2003; Jian et al., 2003; Peng et al., 2006). Our new geochronological data show that the volcanic rocks in the Xiaodingxi and Manghuihe sequences erupted at 210–214 Ma, about 20 Ma later than the syn-collisional Manghuai volcanic rocks. This time gap is consistent with a post-collisional magmatic setting (e.g. volcanic eruptions), which is usually 15–20 Ma after the syn-collisional event (Liegeois, 1998; Coulon et al., 2002; Cvetković et al., 2004). In addition, the Xiaodingxi and Manghuihe volcanic sequences are overlain with angular unconformity by Late Triassic to Early Jurassic red foreland molasse of the Yiwanshui Formation. This stratigraphic relationship establishes the latest Triassic as the time of collision along the Lancangjiang zone (e.g., Yunnan BGMR, 1990; Zhong, 1998) and places the upper Triassic Xiaodingxi and Manghuihe formations in a post-collisional magmatic setting.

Our geochemical data for the Xiaodingxi and Manghuihe volcanic sequences constrain the geodynamic setting of the Lancangjiang post-collisional magmatism. Group 1 samples are interpreted to be the differentiated product of the primitive high MgO and low Al_2O_3 melts originated from the refractory metasomatized mantle with the involvement of 5–10% pelagic sediments trapped into the source region during subduction. The primary magma for Group 2 samples was derived from a plagioclase-rich, garnet-free source constituted by 15–20% asthenospheric and 80–85% lithospheric components modified by recycled sediment-derived fluids. Group 1 samples show higher (La/Yb)n, (La/Sm)n and Ce/Y ratios than Group 2, suggestive of a deeper melting source than Group 2 (e.g., Deniel, 1998; Espinoza et al., 2005). In addition, the Xiaodingxi sequence is conformably overlain by the Manghuihe Formation (Figs. 1 and 2). The Group 1 samples were mainly collected from the Xiaodingxi sequence and the lower part of the Manghuihe sequence, and Group 2 was collected from the middle–upper part of the Manghuihe sequence. These data

appear to suggest a decrease of melting depth levels and an upward migration of the melting source from Group 1 to Group 2 with time. Therefore, the magmatism might involve a two-stage process: (1) during subduction, the recycled pelagic sediments were firstly incorporated into the overlying mantle forming the Group 1 hybridized source; (2) the recycled sediments were subsequently dehydrated to metasomatize the overlying lithospheric mantle to generate the enriched end-member of the Group 2 source. Such a process developed a metasomatized mantle wedge with lower segment modified by the recycled sediments and middle to upper segments metasomatized by subducted sediment-derived fluids.

It is well known that continuous subduction can result in the HP-UHP metamorphism of the subducted slab to form eclogite, and slab detachment can then be developed due to the density increase of the eclogitic slab (e.g., Cooke and O'Brien, 2001; Bird, 1979). Taking account of the zonal distribution pattern of the Lancangjiang magmatic rocks, we propose that the buoyancy of the asthenospheric mantle in response to the slab detachment (Davis and von Blanckenburg, 1995; Whalen et al., 2006; Orozco-Esquivel et al., 2007) is a potential mechanism governing the genesis of the Groups 1 and 2 rocks. The upwelling of asthenospheric mantle not only supplies heat, but also causes the thermo-mechanical erosion of subduction-modified lithospheric mantle. As a result, the lower segment of the metasomatized wedge was firstly melted to produce the Group 1 parental magma. The appearances of high-pressure blueschist and eclogite along the Lancangjiang suture can be used to constrain the slab detachment depth to less than 60 km and more than 70–80 km, respectively (e.g., Monié and Chopin, 1991; Avigad and Garfunkel, 1991; Davis and von

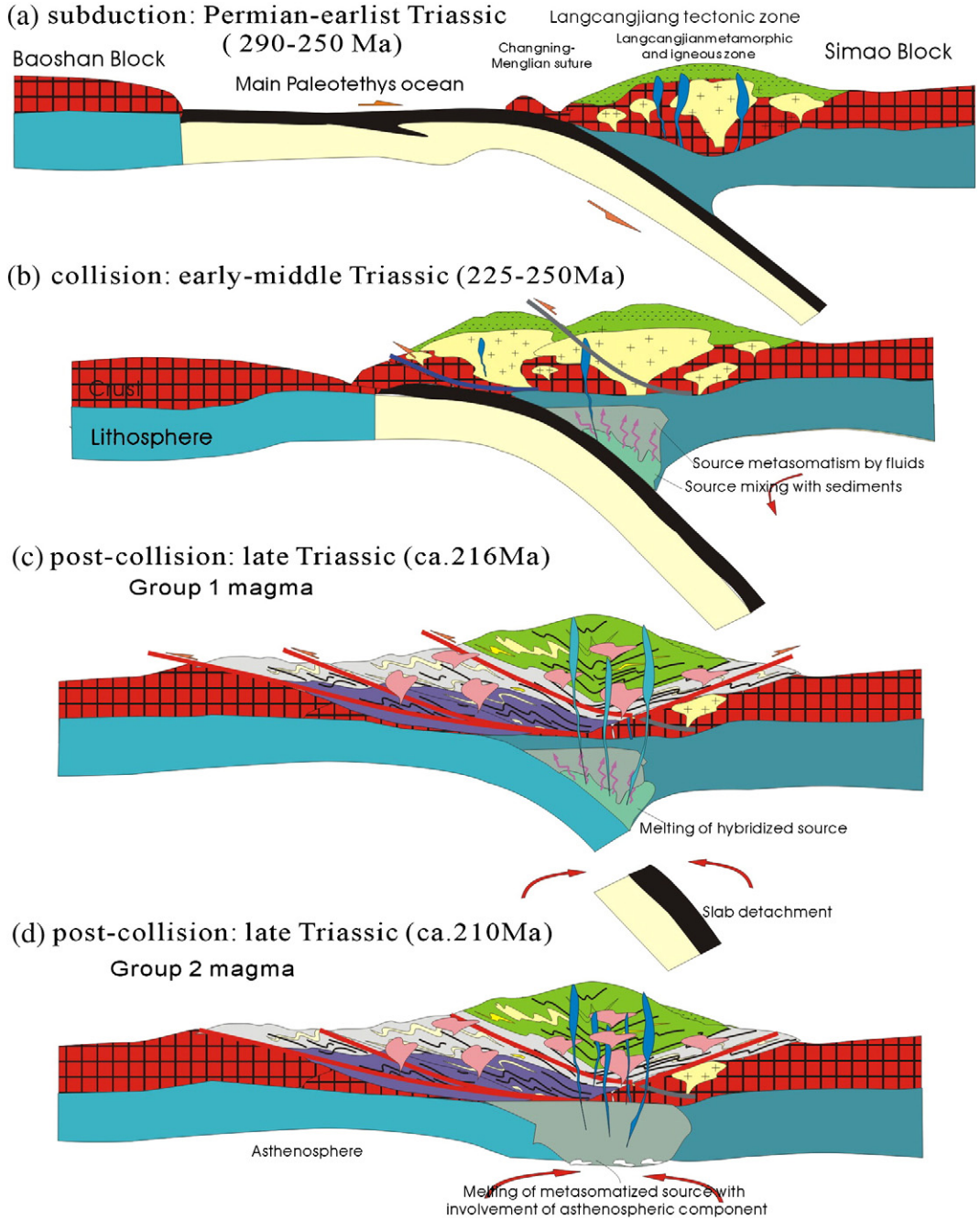

Fig. 11. Schematic tectonic cartoons showing the Paleotethys temporal evolution along the Lancangjiang tectonic zone. (a) The Permian–earliest Triassic (about 290–250 Ma) eastward subduction of the Paleotethys Ocean, (b) early–middle Triassic (about 250–225 Ma) collision of the Simao with Baoshan Blocks, and (c–d) late Triassic (ca. 210–220 Ma) post-collisional stage in response to the initial uprising of asthenospheric mantle shortly after slab detachment (c) and the progressive ascending up to the depth of less than 60 km (d).

Blanckenburg, 1995). Along the Lancangjiang zone, the Shuangjiang blueschist is the only such rock identified during the past decades, pointing to a detachment depth level of less than 60 km. Therefore, we infer that the ascending asthenospheric mantle probably reached a depth of less than 60 km and mixed with fluid-metasomatized wedge to create the hybridized source. This hybridized source was subsequently melted to generate the magma that formed the Group 2 rocks.

Another dispute is whether the main Paleotethys ocean subducted eastward or westward along the Lancangjiang zone (e.g., Yunnan BGMR, 1990; Yang et al., 1994; Fan and Zhang, 1994; Zhong, 1998; Tabakh and Utha-Aroon, 1998; Metcalfe, 2002). In theory, the subduction-affected lithospheric mantle and its melt derivations should be mainly developed in the hanging wall rather than the footwall of the Lancangjiang suture. In the region, the remnants of late Paleozoic oceanic-island basalts are exposed on the west side of the Lancangjiang igneous zone, and the Upper Triassic volcanic sequence are exposed on the east side. The Permian–Triassic blueschist and ophiolitic rocks also occur along the Changning–Menglian areas to the west of the Lancangjiang volcanic zone (Zhang et al., 1993; Zhao et al., 1994; Zhong, 1998). Paired metamorphic belts with a low-P/T metamorphic belt in the east and a high-P/T metamorphic belt in the west, and increasing metamorphic grade eastwards are also documented along this zone (Zhang et al., 1993; Zhong, 1998). Together, these data support eastward subduction for the main Paleotethys ocean, consistent with that in northern Thailand documented by Barr et al. (2006).

Incorporating all the data above and also considering the absence of lower Triassic strata in the study area allow us to propose the following tectonic scenario for the temporal evolution of the Paleotethys along the Lancangjiang tectonic zone as shown in Fig. 11a–d. During the Devonian and Carboniferous, the main Paleotethys ocean spreads to its greatest width along the northern margin of Gondwana. During Permian and earliest Triassic, the ocean subducted eastward beneath the Simao Block along the Lancangjiang tectonic zone (Fig. 11a) and the crustal components have synchronously been trapped into mantle depths. It is developed for the island-arc system and Ailaoshan (SW China) and Nan–Sra (Thailand) back-arc basin along the margin of the Yangtze and Indochina Blocks. In the early–middle Triassic, the Baoshan–Sibumasu Blocks collided with the Simao Block (or western Indochina Block), resulting into the development of the metasomatized mantle wedge and extensive thrusting of the Simao Block over the subducted part of Baoshan Block (Fig. 11b). From the early Late Triassic, the Lancangjiang tectonic zone underwent post-collision extensional collapse in response to uprising of the asthenospheric mantle in response to slab detachment (Fig. 11c–d). The thermo-mechanical erosion of subduction-modified lithospheric mantle by the upwelling asthenospheric mantle induced partial melting of lower segment of the metasomatized wedge to form Group 1 primary magmas (Fig. 11c) and subsequently melting of the upper segments of the metasomatized wedge to generate the Group 2 magma (Fig. 11d).

Supplementary materials related to this article can be found online at doi:10.1016/j.lithos.2010.09.012.

Acknowledgements

We are grateful to Profs. Andrew Kerr, Bernd Lehmann and another anonymous reviewer for their critical and constructive review and comments on this paper. We would like to thank Prof. Peter A. Cawood for polishing the English and constructive reviews. This study was financially supported by projects from the China Natural Science Foundation (40830319 and 40825009), the National Basic Research Program of China (2007CB411403), the Chinese Academy of Science (KZCX1-YW-15-1 and KZCX2-YW-128), and the China Petroleum and Chemical Corporation grants (08YPH004). This is a contribution to Guangzhou Institute of Geochemistry, the Chinese Academy of Sciences.

References

Acharyya, S.K., 1998. Break-up of the greater Indo-Australian continent and accretion of blocks framing south and East Asia. Journal of Geodynamics 26 (1), 149–170.
Avigad, D., Garfunkel, Z., 1991. Uplift and exhumation of high-pressure metamorphic terrains: the example of the Cycladic blueschist belt (Aegean Sea). Tectonophysics 188, 357–372.
Baker, D.R., Eggler, D.H., 1983. Fractionation paths of Atka (Aleutians) high-alumina basalts: constraints from phase relations. Journal of Volcanology and Geothermal Research 18, 387–404.
Barr, S.M., Macdonald, A.S., Dunning, D.R., Ounchanum, P., Yaowanoiyothin, W., 2000. U–Pb (zircon) age, and Paleotectonic setting of the Lampang volcanic belt, Northern Thailand. Journal of Geology Society, London 157, 553–563.
Barr, S.M., MacDonald, A.S., Ounchanum, P., Hamilton, M.A., 2006. Age, tectonic setting and regional implications of the Chiang Khong volcanic suite, northern Thailand. Journal of the Geology Society 163, 1037–1046.
Bartels, K.S., Kinzler, R.J., Grove, T.L., 1991. High pressure phase relation of primitive high-alumina basalt from Medicine Lake volcano, northern California. Contributions to Mineralogy and Petrology 108, 253–270.
Ben Othman, D., White, W.M., Patchett, J., 1989. The geochemistry of marine sediments, island arc magma genesis, and crust–mantle recycling. Earth and Planetary Science Letters 94, 1–21.
Bird, P., 1979. Continental delamination and the Colorado Plateau. Journal of Geophysical Research 84, 7561–7571.
Brophy, J.G., 1988. Basalt convection and plagioclase retention: a model for the generation of high-Al basalt. Journal of Geology 97, 319–329.
Brophy, J.G., Marsh, B.D., 1986. On the origin of high-Al arc basalt and the mechanics of melt extraction. Journal of Petrology 27, 763–789.
Bullard, E.C., Everett, J.E., Smith, A.G., 1965. The fit of the continents around the Atlantic: a symposium on continental drift. Philosophical Transactions of the Royal Society of London. Series A 258, 41–51.
Cobbing, E.J., Pitfield, P.E., Darbyshire, D.P.F., Mallick, D.I.J., 1992. The granites of the South-East Asian Tin Belt. Overseas Memoir of the British Geological Survey 10, 1–369 Her Majesty's Sth Off, Norfolk, England.
Cooke, R.A., O'Brien, P.J., 2001. Resolving the relationship between high P–T rocks and gneisses in collisional terrane: an example from the Gföhl gneiss–granulite association in the Moldanubian Zone, Austria. Lithos 58, 33–54.
Coulon, C., Megartsi, M., Fourcade, S., 2002. Post-collisional transition from calc-alkaline to alkaline volcanism during the Neofene in Oranie (Algerua): magmatic expression of a slab breakoff. Lithos 62, 87–110.
Crawford, A.J., Falloon, T.J., Green, D.H., 1989. Classification, petrogenesis and tectonic setting of boninites. In: Crawford, A.J. (Ed.), Boninites and Related Rocks. Unwin Hyman, London, pp. 1–49.
Cvetković, V., Prelević, D., Downes, H., Jovanović, M., Vaselli, O., Pécskay, Z., 2004. Origin and geodynamic significance of Tertiary postcollisional basaltic magmatism in Serbia (central Balkan Peninsula). Lithos 73, 161–186.
Davis, J.H., von Blanckenburg, F., 1995. Slab breakoff: a model of lithosphere detachment and its test in the magmatism and deformation of collisional orogens. Earth and Planetary Science Letters 129, 85–102.
Defant, M.J., Drummond, M.S., 1990. Derivation of some modern arc magmas by melting of young subducted lithosphere. Nature 347, 662–665.
Deniel, C., 1998. Geochemical and isotopic (Sr, Nd, Pb) evidence for plume–lithosphere interactions in the genesis of Grande Comore magmas (Indian Ocean). Chemical Geology 144, 281–303.
Espinoza, F., Morata, D., Pelleter, E., Maury, R.C., Suarez, M., Lagabrielle, Y., Polve, M., Bellon, H., Cotton, J., De la Cruz, R., Guivel, C., 2005. Petrogenesis of the Eocene and Mio–Pliocene alkaline basaltic magmatism in Meseta Chile Chico, southern Patagonia, Chile: evidence for the participation of two slab windows. Lithos 82, 315–343.
Falloon, T.J., Green, D.H., 1987. Anhydrous partial melting of MORB pyrolite and other peridotite compositions at 10 kbar: implications for the origin of primitive MORB glass. Mineral Petrology 37, 181–219.
Fan, C.J., Zhang, Y.F., 1994. The structure and tectonics of western Yunnan. Journal of Southeast Asian Earth Sciences 9 (4), 355–361.
Fan, W.M., Wang, Y.J., Zhang, A.M., Zhang, F.F., Zhang, Y.Z., 2010. Permian arc-back-arc basin development along the Ailaoshan tectonic zone: geochemical, isotopic and geochronological evidences from the Mojiang volcanic rocks, Southwest China. Lithos 119, 553–568.
Feng, Q.L., 2002. Stratigraphy of volcanic rocks in the Changning–Menglian Belt in southwestern Yunnan, China. Journal of Asian Earth Sciences 20 (6), 657–664.
Fontaine, H., 2002. Permian of Southeast Asia: an overview. Journal of Asian Earth Sciences 20 (6), 567–588.
Fournelle, J., Marsh, B.D., 1991. Shisalkin volcano: Aleutian high-Al basalts and the question of plagioclase accumulation. Geology 19, 234–237.
Fujii, T., Scarfe, C.M., 1985. Compositions of liquids coexisting with spinel lherzolite at 10 kbar and the genesis of MORBs. Contributions to Mineralogy and Petrology 90, 18–28.
Gust, D.A., Perfit, M.R., 1987. Phase relations of high-Mg basalt from Aleutian Island Arc: implications for primary island arc basalts and high-Al basalts. Contributions to Mineralogy and Petrology 97, 7–18.
Hart, S.R., 1984. A large-scale isotope anomaly in the Southern Hemisphere mantle. Nature 309, 753–757.

Hart, S.P., 1988. Heterogeneous mantle domains: signature and mixing chronologies. Earth and Planetary Science Letters 90, 273–296.
Hawkesworth, C.J., Rogers, N.W., van Calsteren, P.W.C., Menzies, M.A., 1984. Mantle enrichment processes. Nature 311 (27), 331–335.
Helmcke, D., 1985. The Permo-Triassic 'Paleotethys' in mainland Southeast-Asia and adjacent parts of China. Geologische Rundschau 74, 215–228.
Hemond, C., Devey, C.W., Chauvel, C., 1994. Source compositions and melting processes in the Society and Austral plumes (South Pacific Ocean): element and isotope (Sr, Nd, Pb, Th) geochemistry. Chemical Geology 115, 7–45.
Hennig, D., Lehmann, B., Frei, D., Belyatsky, B., Zhao, X.F., Cabral, A.R., Zeng, P.S., Zhou, M.F., Schmidt, K., 2009. Early Permian seafloor to continental arc magmatism in the eastern Paleo-Tethys: U–Pb age and Nd–Sr isotope data from the southern Lancangjiang zone, Yunnan, China. Lithos 113 (3–4), 408–422.
Hou, Z.Q., Wang, L.Q., Zaw, K., Mo, X.X., Wang, M.J., Li, D.M., Pan, G.T., 2003. Post-collisional crustal extension setting and VHMS mineralization in the Jinshajiang orogenic belt, southwestern China. Ore Geology Review 22, 177–199.
Hsu, K.J., Bernoulli, D., 1978. Genesis of the Tethys and the Mediterranean. Initial Reports of the Deep Sea Drilling Project 42 (1), 943–949.
Hutchison, C.S., 1989. Geological Evolution of Southeast Asia. Clarendon, Oxford, pp. 1–368.
Jian, P., Wang, X., He, L., Wang, C., 1998. U–Pb zircon dating of the Shuanggou ophiolite from Xinping County, Yunnan Province. Acta Petrologica Sinica 58, 1–17 (in Chinese with English abstract).
Jian, P., Liu, D.Y., Sun, X.M., 2003. SHRIMP dating of Baimaxueshan and Ludian granitoid batholiths Northwestern Yunnan Province, and its geological implications. Acta Geoscientia Sinia 24 (4), 338–342 (in Chinese with English abstract).
Jian, P., Liu, D.Y., Sun, X.M., 2004. SHRIMP dating of Jicha Alaskan-type gabbro in western Yunnan Province: evidence for the early Permian subduction. Acta Geologica Sinica 78, 165–170.
Jian, P., Liu, D.Y., Sun, X.M., 2008. SHRIMP dating of the Permo-Carboniferous Jinshajiang ophiolite, southwestern China: geochronological constraints for the evolution of Paleotethys. Journal of Asian Earth Sciences 32, 371–384.
Jian, P., Liu, D.Y., Kröner, A., Zhang, Q., Wang, Y.Z., Sun, X.M., Zhang, W., 2009. Devonian to Permian plate tectonic cycle of the Paleo-Tethys Orogen in southwest China (II): insights from zircon ages of ophiolites, arc/back-arc assemblages and within-plate igneous rocks and generation of the Emeishan CFB province. Lithos 13 (3–4), 767–784.
Johnston, A.D., 1986. Anhydrous P–T phase relations of near-primary high-Al basalt from the South Sandwich Islands: implications for the origin of island arcs and tonalite–trondhjemite series rocks. Contributions to Mineralogy and Petrology 92, 368–382.
Kelemen, P.B., 1995. Genesis of high Mg andesites and the continental crust. Contributions to Mineralogy and Petrology 120, 1–19.
Kersting, A.B., Arculus, R.J., 1994. Klyuchevskoy volcano, Kamchatka, Russia: the role of high-flux recharged, tapped and fractionated magma chambers in the genesis of high Al_2O_3 from high-MgO basalt. Journal of Petrology 35, 1–41.
Liegeois, L.P., 1998. Preface: some words on the post-collisional magmatism. Lithos 45 (XV-XVII).
Liu, B.P., 1993. Tectonic evolution of Paleo-Tethys poly-island-ocean in Changning–Menglian and Lancangjiang belts, Southwestern Yunnan, China. Earth Science 18 (5), 529–538.
Liu, C.S., Zhu, J., Xu, X.S., 1989. Study on the characteristics of Lincang composite granite batholith in west Yunnan. Geology of Yunnan 8 (3–4), 189–204.
Ludwig, K.R., 2001. Using Isoplot/EX, version 2.49. In: A Geochronological toolkit for Microsoft Excel, Berkeley Geochronological Center Special Publication, Berkeley, pp. 1–55.
Luhr, J.F., Haldar, D., 2006. Barren Island Volcano (NE Indian Ocean): island-arc high-alumina basalts produced by troctolite contamination. Journal of Volcanology and Geothermal Research 149, 177–212.
Lytwyn, J., Rutherford, E., Burke, K., Xia, C., 2001. The geochemistry of volcanic, plutonic and turbiditic rocks from Sumba, Indonesia. Journal of Asian Earth Sciences 19, 481–500.
Ma, C.Q., Li, Z.C., Ehlers, C., 1998. A post-collisional magmatic plumbing system: Mesozoic granitoid plutons from the Dabieshan high-pressure and ultrahigh-pressure metamorphic zone, East-central China. Lithos 45, 431–456.
Macdonald, A.S., Barr, S.W., 1978. Tectonic significance of Late Carboniferous volcanic arc in Northern Thailand. Proceedings of the third regional conference on geology and mineral resources of Southeast Asia, Bangkok, Thailand, pp. 151–156.
Marsh, B.D., 1976. Some Aleutian andesites: their nature and source. Journal of Geology 84, 27–45.
Metcalfe, I., 1996. Gondwanaland dispersion, Asian accretion and evolution of eastern Tethys. Australian Journal of Earth Sciences 43 (6), 605–623.
Metcalfe, I., 2002. Permian tectonic framework and palaeogeography of SE Asia. Journal of Asian Earth Sciences 20, 551–566.
Michard, A., Montigny, R., Schlich, R., 1986. Geochemistry of the mantle beneath the Rodriguez Triple Junction and the South-East Indian Ridge. Earth and Planetary Science Letters 78, 104–114.
Mo, X.X., Shen, S.Y., Zhu, Q.W., 1998. Volcanics-Ophiolite and Mineralization of Middle and Southern Part in Sanjiang, Southern China. Geological Publishing House, Beijing, pp. 1–128 (in Chinese).
Monié, P., Chopin, C., 1991. $^{40}Ar/^{39}Ar$ dating in coesite-bearing and associated units of the Dora Maira massif, Western Alps. European Journal of Mineralogy 3, 239–262.
Morra, V., Secchi, F.A.G., Melluso, L., Franciosi, L., 1997. High-Mg subduction-related Tertiary basalts in Sardinia, Italy. Lithos 40, 69–91.
Myers, J.D., 1988. Possible petrogenetic relations between low- and high-MgO Aleutian basalts. Geological Society American Bulletin 100, 1040–1053.
Myers, J.D., Johnston, A.D., 1996. Phase equilibria constraints on models of subduction zone magmatism. In: Bebout, G.E., Scholl, D.W., Kirby, S.H., Platt, J.P. (Eds.), Subduction: Top to Bottom. American Geophysical Union, Washington, DC, pp. 229–249.
Orberger, B., Lorand, J.P., Girardeau, J., Mercier, J.C., Pitragool, S., 1995. Petrogenesis of ultramafic rocks and associated chromitites in the Nan Uttaradit ophiolite, Northern Thailand. Lithos 35, 153–182.
Orozco-Esquivel, T., Petrone, C.M., Ferrari, L., Tagami, T., Manetti, P., 2007. Geochemical and isotopic variability in lavas from the eastern Trans-Mexican Volcanic Belt: slab detachment in a subduction zone with varying dip. Lithos 93, 149–174.
Oźerov, A., 2000. The evolution of high-alumina basalts of the Klyuchevskoy volcano, Kamchatka, Russia, based on microprobe analyses of mineral inclusions. Journal of Volcanology and Geothermal Research 95, 65–79.
Panjasawatwong, Y., Zaw, K., Chantaramee, S., Limtrakun, P., Pirarai, K., 2006. Geochemistry and tectonic setting of the Central Loei volcanic rocks, Pak Chom area, Loei, northeastern Thailand. Journal of Asian Earth Sciences 26, 77–90.
Pearce, J.A., Baker, P.E., Harvey, P.K., Luff, I.W., 1995. Geochemical evidence for subduction fluxes, mantle melting and fractional crystallization beneath the South Sandwich Island arc. Journal of Petrology 36, 1073–1109.
Peng, T.P., Wang, Y.J., Fan, W.M., Liu, D.Y., Shi, Y.R., Miao, L.C., 2006. SHRIMP zircon U–Pb geochronology of early Mesozoic felsic igneous rocks from the southern Lancangjiang and its tectonic implications. Science in China (Series D) 49, 1032–1042.
Peng, T.P., Wang, Y.P., Zhao, G.C., Fan, W.M., Peng, B.X., 2008. Arc-like volcanic rocks from the southern Lancangjiang zone, SW China: geochronological and geochemical constraints on their petrogenesis and tectonic implications. Lithos 102, 358–373.
Perfit, M.R., Gust, D.A., Bence, A.E., Arculus, R.J., Taylor, S.R., 1980. Geochemical characteristics of island-arc basalts: implications for mantle sources. Chemical Geology 30, 227–256.
Phajuy, B., Panjasawatwong, Y., Osataporn, P., 2005. Preliminary geochemical study of volcanic rocks in the Pang Mayao area, Phrao, Chiang Mai, northern Thailand: tectonic setting of formation. Journal of Asian Earth Sciences 24, 765–776.
Rapp, R.P., Watson, E.B., Miller, C.F., 1991. Partial melting of amphibolite/eclogite and the origin of Archean trondhjemites and tonalites. Precambrian Research 51, 1–25.
Rehkämper, M., Hofmann, A.W., 1997. Recycled ocean crust and sediment in Indian Ocean MORB. Earth and Planetary Science Letters 147, 93–106.
Rivalenti, G., Mazzucchelli, M., Girardi, V.A.V., Cavazzini, G., Finatti, C., Barbieri, M.A., Teixeira, W., 1998. Petrogenesis of the Plaeoproterozoic basalt–andesite–rhyolite dyke association in the Carajás region, Amazonian craton. Lithos 43, 235–265.
Schiano, P., Clocchiatti, R., Boivin, P., Medard, E., 2004. The nature of melt inclusions inside minerals in an ultramafic cumulate from Adak volcanic center, Aleutian Arc: implications for the origin of high-Al basalts. Chemical Geology 203, 169–179.
Sengor, A.M.C., 1979. Mid-Mesozoic closure of Permo-Triassic Tethys and its implications. Nature 279, 390–593.
Sengor, A.M.C., Hsu, K.J., 1984. The Cimmerides of eastern Asia history of the eastern end of Paleo-Tethys. Me'moires de la Socie'ti Giologique de France, Nouvelle Sirie 147, 139–167.
Shen, S.Z., Shi, G.R., Fang, Z.J., 2002. Permian Bra Chiopods from the Baoshan and Simao Blocks in Western Yunnan, China. Journal of Asian Earth Sciences 20, 665–682.
Shimoda, G., Tatsumi, Y., Nohda, S., Ishizaha, K., Jahn, B.M., 1998. Setouchi high-Mg andesites revisited: geochemical evidence for melting of subducting sediments. Earth and Planetary Science Letters 160, 479–492.
Shinjo, R., Chung, S.L., Kato, Y., Kimura, M., 1999. Geochemical and Sr-Nd isotopic characteristics of volcanic rocks from the Okinwa Trough and Ryukyu Arc: implications for the evolution of a young, intracontinental back arc basin. Journal Geophysical Research 104 (B5), 10591–10608.
Sobolev, A.V., Hofmann, A.W., Nikogosian, I.K., 2000. Recycled oceanic crust observed in ghost plagioclase within the source of Mauna Loa Lavas. Nature 404 (27), 986–990.
Sone, M., Metcalfe, I., 2008. Parallel Tethyan sutures in mainland Southeast Asia: New insights for Palaeo-Tethys closure and implications for the Indosinian orogeny. Comptes Rendus Geoscience 340, 166–179.
Song, B., Zhang, Y.H., Wang, Y.S., 2002. Mount making and procedure of the SHRIMP dating. Geology Review 48, 26–30.
Stolz, A.J., Vame, R., Davies, G.R., Wheller, G.E., Foden, J.D., 1990. Magma source components in an arc-continent collision zone: the Flores–Lembata sector, Sunda Arc, Indonesia. Contributions to Mineralogy and Petrology 105, 585–601.
Sun, S.S., McDonough, W.F., 1989. Chemical and isotopic systematics of oceanic basalts: implications for mantle composition and processes. In: Saunders, A.D., Norry, M.J. (Eds.), Magmatism in the Ocean Basins: Geological Society of London, Special Publications, 42, pp. 313–345.
Tabakh, M.E., Utha-Aroon, C., 1998. Evolution of Permian carbonate platform to siliciclastic basin: Indochina plate, Thailand. Sedimentary Geology 121, 97–119.
Taylor, S.R., McLennan, S.M., 1985. The continental crust: Its composition and evolution. Oxford Press Blackwell, pp. 1–312.
Tulyatid, J., Charusiri, P., 1999. The ancient Tethys in Thailand as indicated by nationwide airborne geophysical data, Chiang Mai. International Symposium Shallow Tethys 5, 335–352.
Ueno, Katsumi, Hisada, Ken-ichiro, 2001. The Nan-Uttaradit-Sa Kaeo Suture as a main Paleo-Tethyan Suture in Thailand: is it real? Gondwana Research 4 (4), 804–806.
Vroon, P.Z., van Bergen, M.J., White, W.M., Varekamp, J.C., 1993. Sr–Nd–Pb isotope systematics of the Banda arc, Indonesia: combined subduction and assimilation of continental material. Journal of Geophysical Research 98, 22349–22366.
Vroon, P.Z., van Bergen, M.J., Klaver, G.J., White, W.M., 1995. Strontium, neodymium, and lead isotopic and trace-element signature of the East Indonesian sediments: provenance and implications for Banda Arc magma genesis. Geochemica et Cosmochimica Acta 59, 2573–2598.
Wang, Y.J., Fan, W.M., Zhang, Y.H., Peng, T.P., Chen, X.Y., Xu, Y.G., 2006. Kinematics and $^{40}Ar/^{39}Ar$ geochronology of the Gaoligong and Chongshan shear systems, western Yunnan, China: implication for early Oligocene tectonic extrusion of SE Asia. Tectonophysics 418 (3–4), 235–254.

Whalen, J.B., McNicoll, V.J., van Staal, C.R., Lissenberg, C.J., Longstaffe, F.J., Jenner, G.A., van Breeman, O., 2006. Spatial, temporal and geochemical characteristics of Silurian collision-zone magmatism Newfoundland Appalachians: an example of a rapidly evolving magmatic system related to slab break-off. Lithos 89 (3–4), 377–404.

Williams, I.S., Claesson, S., 1987. Isotope evidence for the Precambrian province and Caledonian metamorphism of high-grade paragneiss from the Seve Nappes, Scandinavian Caledonides, II. Ion microprobe zircon U–Th–Pb. Contributions to Mineralogy and Petrology 97, 205–217.

Wu, H.R., Boulter, C.A., Baojia, Ke., Stow, D.A.V., Wang, Z.C., 1995. The Changning–Menglian suture zone, a segment of the major Cathaysian–Gondwana Divide in Southeast Asia. Tectonophysics 242, 267–280.

Yang, K., Mo, X., Zhu, Q., 1994. Tectono-volcanic belts and late Paleozoic–early Mesozoic evolution of south western Yunnan, China. Journal of Southeast Asian Sciences 10 (3/4), 245–262.

Yu, S.Y., Li, K.Q., Shi, Y.P., Zhang, H.H., 2003. A study on the granodiorite in the middle part of Lincang granite batholith. Yunnan Geology 22 (4), 426–442.

Yunnan BGMR (Yunnan Bureau Geological Mineral Resource),1996. Stratigraphy (Lithostratic) of Yunnan Province. China University of Geosciences Press, Wuhan, pp. 1–379 (in Chinese).

Yunnan BGMR (Yunnan Bureau Geological Mineral Resource),1990. Regional Geology of Yunnan Province. Geology Publishing House, Beijing, pp. 1–729 (in Chinese).

Zhang, R., Cong, B., Maruyama, S., Liou, J.G., 1993. Metamorphism and tectonic evolution of the Lancang paired metamorphic belts, southwestern China. Journal of Metamorphic Geology 11, 605–619.

Zhang, H.F., Zhang, B.R., Zhao, Z., Luo, T., 1996. Continental crust subduction and collision along Shangdan tectonic belt of east Qinling: evidence from Pb, Nd and Sr isotopes of granitoids. Science in China, Series D, Earth Science 39, 273–282.

Zhang, H.F., Gao, S., Zhong, Z.Q., Zhang, B.R., Zhang, L., Hu, S.H., 2002. Geochemical and Sr–Nd–Pb isotopic compositions of Cretaceous granitoids: constrains on tectonic framework and crustal structure of the Dabieshan ultrahigh-pressure metamorphic belt, China. Chemical Geology 186, 281–299.

Zhao, J., Zhong, D., Wang, Y., 1994. Metamorphism of Lancang Metamorphic Belt, the western Yunnan and its relation to deformation. Acta Petrologica Sinica 10, 27–40 (in Chinese, with English abstract).

Zhong, D.L., 1998. The Paleotethys Orogenic Belt in West of Sichuan and Yunnan. Science Publishing House, Beijing, pp. 1–230 (in Chinese).

Zimmer, M., Kröner, A., Jochum, K.P., Reischmann, T., Todt, W., 1995. The Gabal Gerf complex: a Precambrian N-MORB ophiolite in the Nubian Shield, NE African. Chemical Geology 123, 29–51.

Zou, H.B., Zindler, A., Xu, X.S., 2000. Major, trace element, and Nd, Sr and Pb studies of Cenozoic basalts in SE China: mantle sources, regional variations and tectonic significance. Chemical Geology 171, 33–47.